Chapter 6

Quasi-geostrophic Analysis

A primary goal of dynamic meteorology is to interpret the observed structure of large-scale atmospheric motions in terms of the physical laws governing the motions. These laws, which express the conservation of momentum, mass, and energy, completely determine the relationships among the pressure, temperature, and velocity fields. As we saw in Chapter 2, these governing laws are quite complicated even when the hydrostatic approximation (which is valid for all large-scale meteorological systems) is applied. For extratropical synoptic-scale motions, however, the horizontal velocities are approximately geostrophic (see Section 2.4). Such motions, which are usually referred to as *quasi-geostrophic*, are often simpler to analyze than are tropical disturbances or planetary-scale disturbances. They are also the major systems of interest in traditional short-range weather forecasting, and are thus a reasonable starting point for dynamical analysis.

In addition to the observation that extratropical weather systems are nearly geostrophic and hydrostatic, we found in the linear wave analyses of Chapter 5 that the properties of Rossby waves resemble these weather systems, whereas those of inertia–gravity waves do not. Specifically, Rossby waves have relatively slow phase speeds and nonzero potential vorticity, whereas the inertia–gravity waves are fast moving and have little or no potential vorticity. We will exploit these properties here in order to filter the full equations to a simpler set, the quasi-geostrophic (QG) equations. Before developing this system of equations, it is useful to briefly summarize the observed structure of midlatitude synoptic systems and the mean circulations in which they are embedded. We then develop the QG equations using potential vorticity and potential temperature, which provides one framework ("*PV Thinking*") for understanding. A second framework for dynamics ("*w Thinking*") is based on the diagnosis of vertical motion through an *"omega equation,"* and will also be thoroughly explored.

6.1 THE OBSERVED STRUCTURE OF EXTRATROPICAL CIRCULATIONS

Atmospheric circulation systems depicted on a synoptic chart rarely resemble the simple circular vortices discussed in Chapter 3. Rather, they are generally

An Introduction to Dynamic Meteorology. DOI: 10.1016/B978-0-12-384866-6.00006-4

highly asymmetric in form, with the strongest winds and largest temperature gradients concentrated along narrow bands called *fronts*. Also, such systems generally are highly baroclinic; the amplitudes and phases of the geopotential and velocity perturbations both change substantially with height. Part of this complexity is due to the fact that these synoptic systems are not superposed on a uniform mean flow, but are embedded in a slowly varying planetary scale flow that is itself highly baroclinic. Furthermore, this planetary scale flow is influenced by *orography* (i.e., by large-scale terrain variations) and continent-ocean heating contrasts so that it is highly longitude dependent. Therefore, while viewing synoptic systems as disturbances superposed on a zonal flow that varies only with latitude and height is a useful first approximation in theoretical analyses (see, e.g., Chapter 7), more complete descriptions require the observed zonal asymmetry.

Zonally averaged cross-sections do provide some useful information on the gross structure of the planetary scale circulation in which synoptic-scale eddies are embedded. Figure 6.1 shows meridional cross-sections of the longitudinally averaged zonal wind and temperature for the solstice seasons of (a) December, January, and February (DJF) and (b) June, July, and August (JJA). These sections extend from approximately sea level (1000 hPa) to about 32 km altitude (10 hPa). Thus, the troposphere and lower stratosphere are shown. This chapter is concerned with the structure of the wind and temperature fields in the troposphere, and the stratosphere is discussed in Chapter 12.

The average pole to equator temperature gradient in the Northern Hemisphere troposphere is much larger in winter than in summer. In the Southern Hemisphere the difference between summer and winter temperature distributions is smaller, due mainly to the large thermal inertia of the oceans, together with the greater fraction of the surface that is covered by oceans in the Southern Hemisphere. Since the mean zonal wind and temperature fields satisfy the thermal wind relationship to a high degree of accuracy, the seasonal cycle in zonal wind speeds is similar to that of the meridional temperature gradient. In the Northern Hemisphere the maximum zonal wind speed in the winter is twice as large as in the summer, whereas in the Southern Hemisphere the difference between winter and summer zonal wind maxima is much smaller. Furthermore, in both seasons the core of maximum zonal wind speed (called the mean jet stream axis) is located just below the *tropopause* (the boundary between the troposphere and stratosphere) at the latitude where the thermal wind integrated through the troposphere is a maximum. In both hemispheres, this is about 30° latitude during winter, but moves poleward to about 45° during summer.

The zonally averaged meridional cross-sections of Figure 6.1 are not representative of the mean wind structure at all longitudes, which can be seen in the distribution of the time-averaged zonal wind component for DJF on the 200-hPa surface in the Northern Hemisphere (Figure 6.2). It is clear that at some longitudes there are very large deviations of the time-mean zonal flow from its longitudinally averaged distribution. In particular, there are strong zonal wind

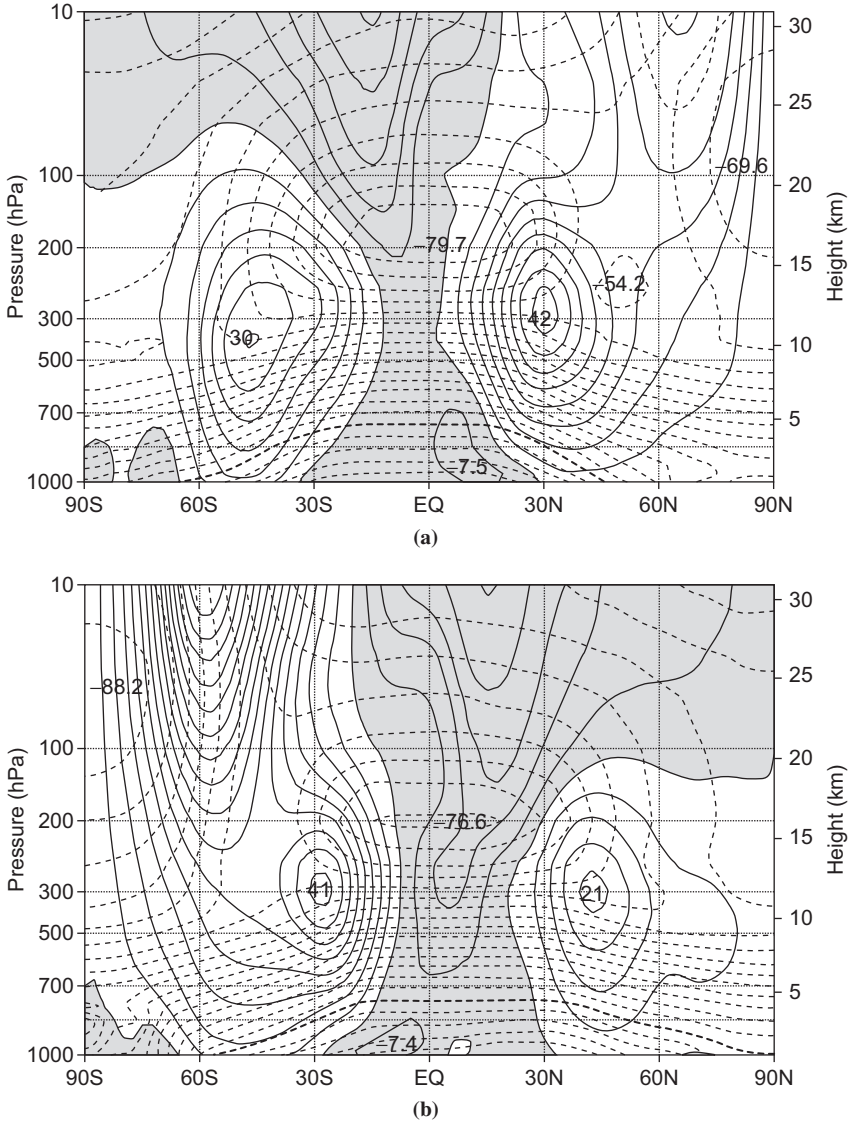

FIGURE 6.1 Meridional cross-sections of longitudinally and time-averaged zonal wind (*solid contours*, interval of 5 m s^{-1}) and temperature (*dashed contours*, interval of 5 K) for December–February (a) and June–August (b). Easterly winds are *shaded* and 0°C isotherm is *darkened*. Wind maxima shown in m s^{-1}, temperature minima shown in °C. (*Based on NCEP/NCAR reanalyses; after Wallace, 2003*.)

maxima (jets) near 30°N just east of the Asian and North American continents and north of the Arabian peninsula; distinct minima occur in the eastern Pacific and eastern Atlantic. Synoptic-scale disturbances tend to develop preferentially in the regions of maximum time-mean zonal winds associated with the western

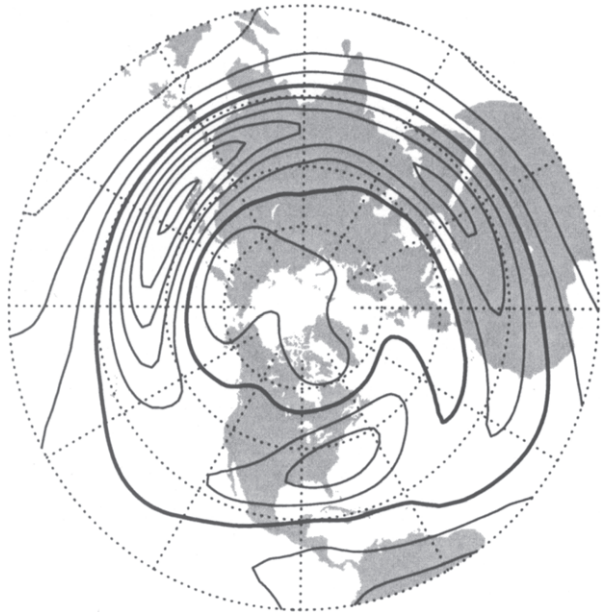

FIGURE 6.2 Mean zonal wind at the 200-hPa level for December through February, averaged for years 1958–1997. Contour interval 10 m s^{-1} (heavy contour, 20 m s^{-1}). (*Based on NCEP/NCAR reanalyses; after Wallace, 2003.*)

Pacific and western Atlantic jets and to propagate downstream along *storm tracks* that approximately follow the jet axes.

The large departure of the northern winter climatological jet stream from zonal symmetry can also be readily inferred from examination of Figure 6.3, which shows the mean 500-hPa geopotential contours for January and July in the Northern Hemisphere. Striking departures from zonal symmetry are apparent, which are linked to the distributions of continents and oceans. The most prominent asymmetries are the troughs in January to the east of the American and Asian continents. Referring to Figure 6.2, we see that the intense jet at 35°N and 140°E is a result of the semipermanent trough in that region. Thus, it is apparent that the mean flow in which synoptic systems are embedded should really be regarded as a longitude-dependent time-averaged flow. In northern summer, 500-hPa geopotential height increases much more over high latitudes as compared to the tropics due to warming in the polar region. As a result, the pole–equator temperature contrast is smaller than in winter, and the height contrast and jet stream are weaker and located at higher latitude.

In addition to its longitudinal dependence, the planetary scale flow also varies from day to day due to its interactions with transient synoptic-scale disturbances. In fact, observations show that the transient planetary scale flow amplitude is comparable to that of the time-mean. As a result, monthly mean

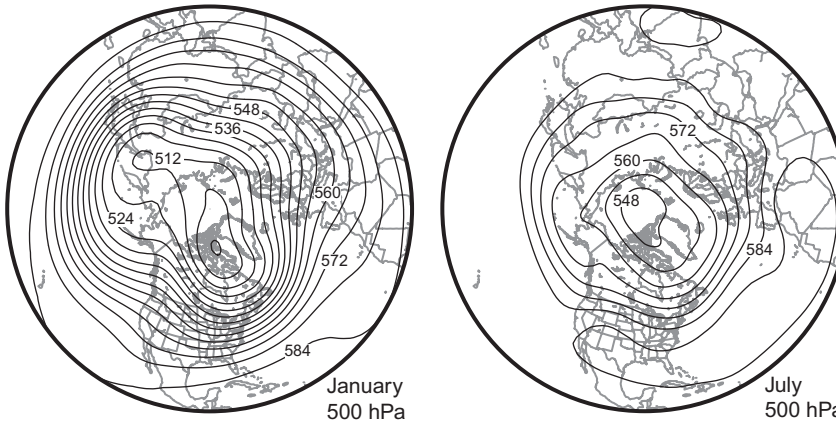

FIGURE 6.3 Mean 500-hPa geopotential height contours in January (*left*) and July (*right*) in the Northern Hemisphere (30-year average). Geopotential height contours are shown every 60 meters. (*Adapted from NOAA/ESRL http://www.esrl.noaa.gov/psd/.*)

charts tend to smooth out the actual structure of the instantaneous jet stream since the position and intensity of the jet vary. Thus, at any time the planetary scale flow in the region of the jet stream has much greater baroclinicity than indicated on time-averaged charts. This point is illustrated schematically in Figure 6.4, which shows a latitude–height cross-section through an observed jet stream over North America. Figure 6.4a shows the zonal wind and potential temperature, whereas Figure 6.4b shows the potential temperature and Ertel potential vorticity. The 2-PVU contour of potential vorticity approximately marks the tropopause. As illustrated in Figure 6.4a, the axis of the jet stream tends to be located above a narrow sloping zone of strong potential temperature gradients called the *polar-frontal* zone. This is the zone that in general separates the cold air of polar origin from warm tropical air. The occurrence of an intense jet core above this zone of large-magnitude potential temperature gradients is, of course, not mere coincidence but rather a consequence of thermal wind balance.

The potential temperature contours in Figure 6.4 illustrate the strong static stability in the stratosphere. They also illustrate the fact that isentropes (constant θ surfaces) cross the tropopause in the vicinity of the jet so that air can move between the troposphere and the stratosphere without diabatic heating or cooling. The strong gradient of Ertel potential vorticity at the tropopause, however, provides a strong resistance to cross-tropopause flow along the isentropes. Note, however, that in the frontal region the potential vorticity surfaces are displaced substantially downward so that the frontal zone is characterized by a strong positive anomaly in potential vorticity associated with the strong relative vorticity on the poleward side of the jet and the strong static stability on the cold air side of the frontal zone.

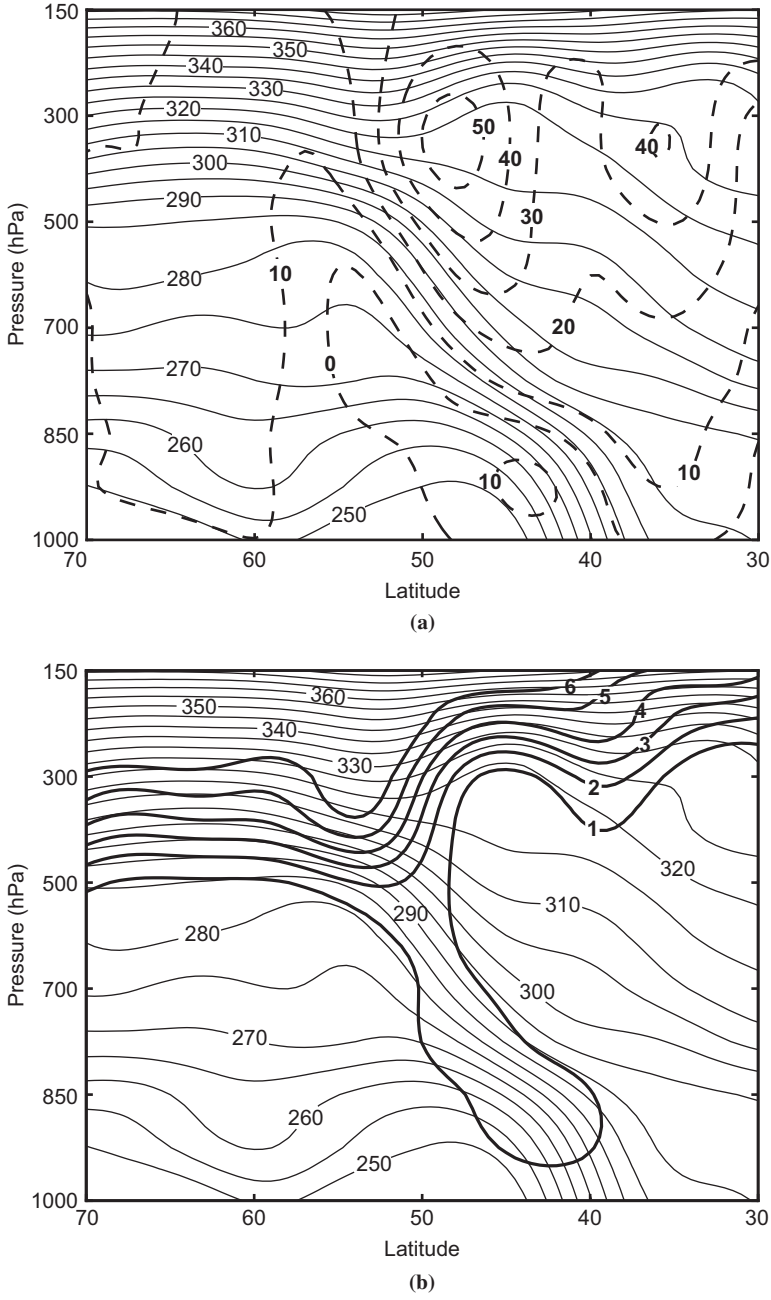

FIGURE 6.4 Latitude–height cross-sections through a cold front at 80W longitude on 2000 UTC January 14, 1999. (a) Potential temperature contours (*thin solid lines*, K) and zonal wind isotachs (*dashed lines*, m s^{-1}). (b) *Thin solid contours* as in (a), *heavy dashed contours*, Ertel potential vorticity labeled in PVU(1-PVU = 10^{-6} K kg^{-1} m^2 s^{-1}).

It is a common observation in fluid dynamics that jets in which strong velocity shears occur may be unstable with respect to small perturbations. Any small disturbance introduced into an unstable jet will tend to amplify, drawing energy from the jet as it grows. For synoptic-scale systems in midlatitudes, the primary instability is called *baroclinic instability* because it depends on the meridional temperature gradient or, equivalently, from thermal-wind balance, on vertical wind shear. Athough horizontal temperature gradients maximize near frontal zones, baroclinic instability is not identical to frontal instability, as most baroclinic instability models describe only geostrophically scaled motions, whereas disturbances in the vicinity of strong frontal zones must be highly ageostrophic. As shown in Chapter 7, baroclinic disturbances may themselves act to intensify pre-existing temperature gradients and thus generate frontal zones.

Disturbances in the midlatitude storm tracks take the form of baroclinic waves and smaller-scale vortices. A statistical analysis of the meridional wind reveals that the baroclinic waves have a dominant wavelength of about 4000 km, and travel eastward at approximately 10 to 15 m s^{-1}(Figure 6.5). The vertical structure of the waves indicates a westward tilt with height in the geopotential height field and, consistent with hydrostatic balance, an eastward tilt with height in the temperature field (Figure 6.6). Vertical motion peaks in the middle troposphere, with rising motion between the trough and ridge and sinking motion west of the trough. It is these organized patterns of vertical motion that are largely responsible for clouds and precipitation in middle latitudes, and understanding the dynamical source for these circulations is a major subject of this chapter. Key aspects of an idealized developing baroclinic system are captured in the schematic vertical cross-section illustrated in Figure 6.7. Throughout the troposphere the trough and ridge axes tilt westward (or upstream) with height,[1] whereas the axes of warmest and coldest air are observed to have the opposite tilt. As will be shown later, the westward tilt of the troughs and ridges is necessary in order that the mean flow transfers potential energy to the developing wave. In the mature stage (not shown in Figure 6.7) the troughs at 500 and 1000 hPa are nearly in phase and, as a consequence, thermal advection and energy conversion are quite weak.

This statistical description of baroclinic waves is manifest in individual realizations of weather disturbances in the form of extratropical cyclones. The stages in the development of a typical extratropical cyclone are shown schematically in Figure 6.8. In the stage of rapid development there is a cooperative interaction between the upper-level and surface flows; strong cold advection is seen to occur west of the trough at the surface, with weaker warm advection to the east. This pattern of thermal advection is a direct consequence of the fact that the trough at 500 hPa lags (lies to the west of) the surface trough so that the mean geostrophic wind in the 1000- to 500-hPa layer is directed across the

[1] As Figure 6.6 reveals, in reality, the phase tilts tend to be concentrated below the 700-hPa level.

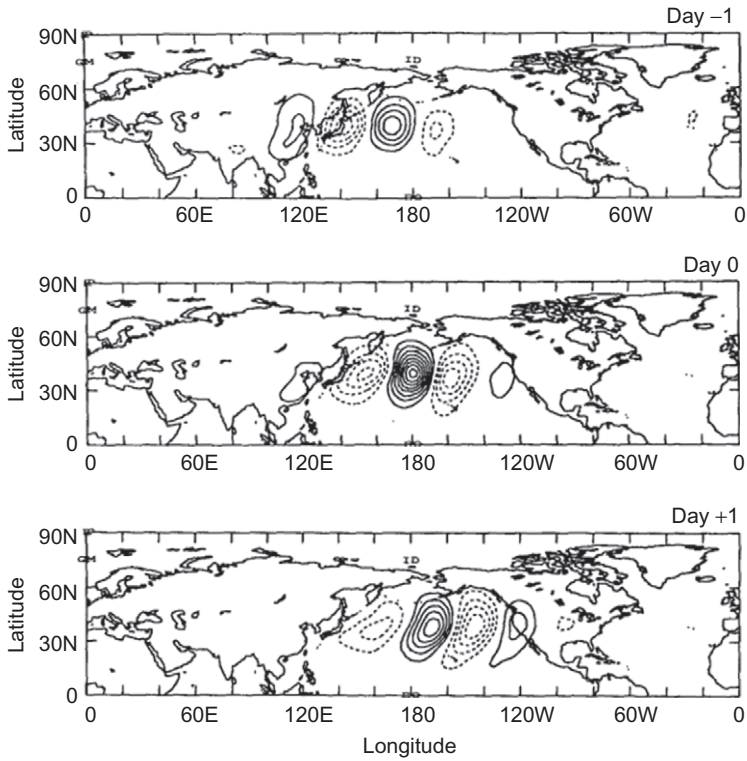

FIGURE 6.5 Linear regression of the meridional wind relative to the base point at 40°N, 180°W. Contours are shown every 2 m s^{-1} with negative values *dashed*. The top, middle, and bottom panels show lags of −1, 0, and +1 days, respectively, relative to the base point, which reveals the motion of the baroclinic waves across the North Pacific ocean. (*After Chang, 1993. Copyright © American Meteorological Society. Reprinted with permission.*)

1000- to 500-hPa thickness lines toward larger thickness west of the surface trough and toward smaller thickness east of the surface trough.

6.2 DERIVATION OF THE QUASI-GEOSTROPHIC EQUATIONS

The main goal of this chapter is to show how the observed structure of midlatitude synoptic systems can be interpreted in terms of the constraints imposed on synoptic-scale motions by the dynamical equations. Specifically, we show that for motions that are nearly hydrostatic and geostrophic, the three-dimensional flow field is determined approximately by the pressure field. Given the small magnitude of vertical motion on these scales, this is a remarkable result. Here we use height, z, as the vertical coordinate, and make the Boussinesq approximation

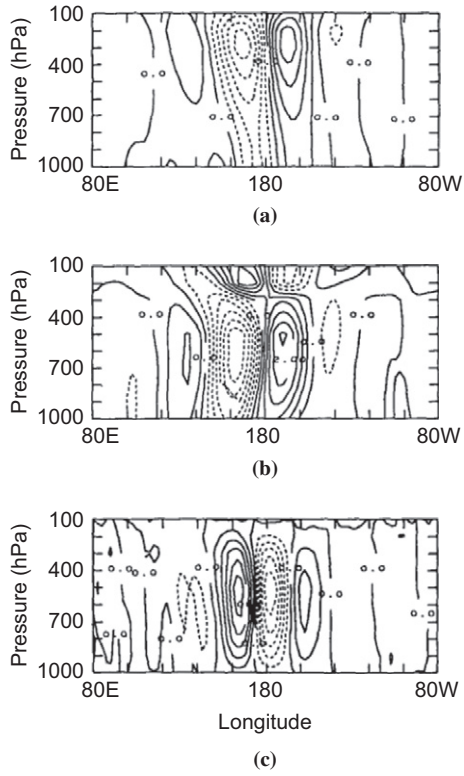

FIGURE 6.6 Linear regression is shown on the longitude–height plane of (a) geopotential height (b) temperature, and (c) vertical motion (ω) relative to the meridional wind at the base point located at 300 hPa, 40°N, and 180°W. Contours are shown every 20 m for geopotential height, 0.5 K for temperature, and 0.02 Pa s^{-1} for vertical motion, with negative values *dashed*. (*After Chang, 1993. Copyright © American Meteorological Society. Reprinted with permission.*) The vertical structure of baroclinic waves is revealed: westward tilt with height for geopotential height anomalies, eastward tilt with height for temperature, and rising motion eastward of the geopotential height trough axis.

so that density is treated as a constant everywhere except for the buoyancy force. This approach has the advantage of simplicity and clarity compared to using pressure as a vertical coordinate, which involves a left-handed coordinate system and reverses the sign of vertical motion (negative is rising). Nevertheless, most weather and climate data are contained in pressure coordinates, so in Section 6.7 we present the isobaric-coordinate form of the equations. For completeness, the isobaric equations also allow for a linear variation of the Coriolis parameter (β-plane approximation), whereas the rest of this chapter employs the f-plane approximation (constant value); this simplifies the analysis and is a good approximation in midlatitudes, since ambient potential vorticity gradients near jet streams are much larger than those of f.

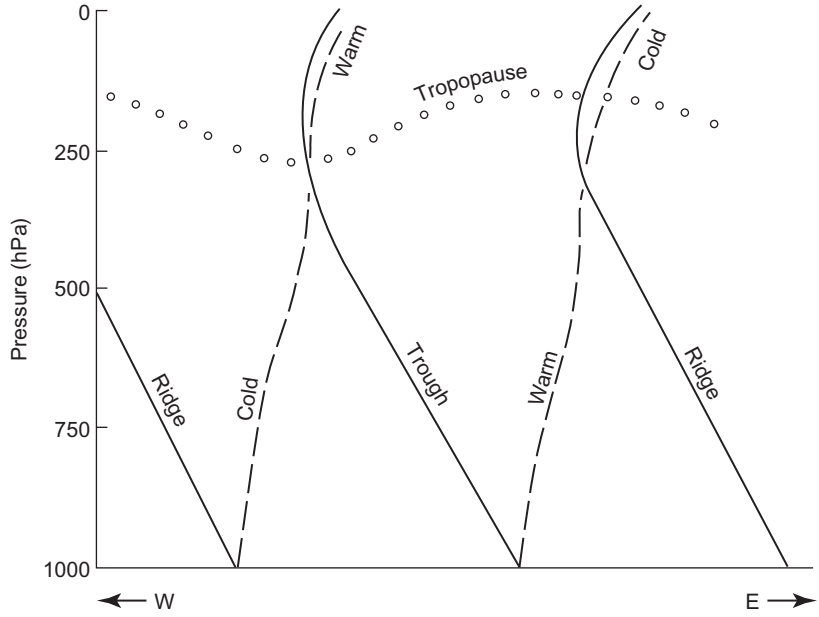

FIGURE 6.7 West–east cross-section through a developing baroclinic wave. *Solid lines* are trough and ridge axes; *dashed lines* are axes of temperature extrema; the chain of *open circles* denotes the tropopause.

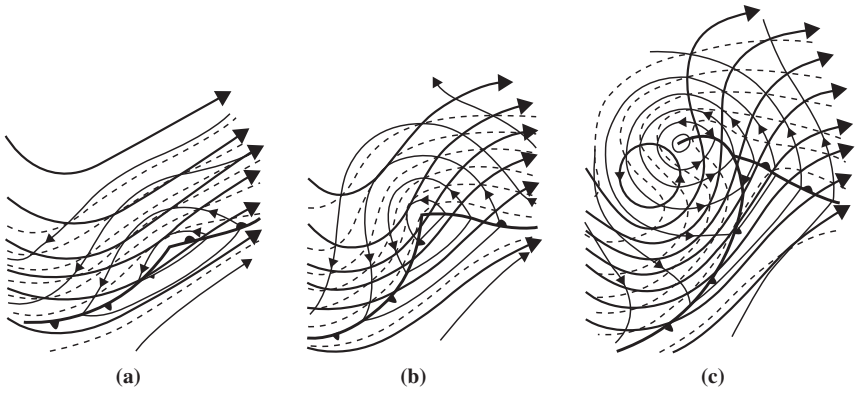

FIGURE 6.8 Schematic 500-hPa contours (*heavy solid lines*), 1000-hPa contours (*thin lines*), and 1000–500-hPa thickness (*dashed lines*) for a developing extratropical cyclone at three stages of development: (a) incipient development stage, (b) rapid development stage, and (c) occlusion stage. (*After Palmén and Newton, 1969.*)

6.2.1 Preliminaries

The geostrophic wind, $\mathbf{V}_g = (u_g, v_g)$ is given by

$$\mathbf{V}_g = \frac{1}{\rho_0 f}\mathbf{k} \times \nabla_h p = \frac{1}{\rho_0 f}\left(-\frac{\partial p}{\partial y}, \frac{\partial p}{\partial x}\right) \tag{6.1}$$

where ρ_0 and f are constants as a result of the Boussinesq and f-plane approximations, respectively. Recall that ∇_h is the horizontal gradient operator $(\frac{\partial}{\partial x}, \frac{\partial}{\partial y})$. The geostrophic relative vorticity, ζ_g, measures the rotational component of the geostrophic wind about the vertical axis,

$$\zeta_g = \frac{\partial v_g}{\partial x} - \frac{\partial u_g}{\partial y} = \frac{1}{\rho_0 f}\nabla_h^2 p \tag{6.2}$$

where the second relationship derives from (6.1); the geostrophic relative vorticity is determined completely by the pressure field.

We will assume that the wind in all but one of the advection terms of the equations may be approximated by the geostrophic wind. The basis for this assumption derives from the following scaling arguments. The Eulerian time tendency and horizontal advection scale like

$$\frac{\partial}{\partial t} + u\frac{\partial}{\partial x} + v\frac{\partial}{\partial y} \sim \frac{U}{L} \tag{6.3}$$

and, for $w \sim Ro\frac{H}{L}U$, vertical advection scales like

$$w\frac{\partial}{\partial z} \sim \frac{U}{L}Ro \tag{6.4}$$

where Ro is the Rossby number, U/fL, discussed in Section 2.4.2. Vertical advection may be neglected for small Rossby number, provided the vertical gradient of the advected quantity is not on the order of Ro^{-1} or larger. Moreover, since the Lagrangian tendency of horizontal momentum scales with the Rossby number, the ageostrophic wind does as well—see (2.24) and (2.25); as a result, the ageostrophic wind is small compared to the geostrophic wind. Therefore, for a small Rossby number, to good approximation we can we make the replacement

$$\frac{D}{Dt} \to \frac{D}{Dt_g} = \frac{\partial}{\partial t} + \mathbf{V}_g \cdot \nabla_h = \frac{\partial}{\partial t} + u_g\frac{\partial}{\partial x} + v_g\frac{\partial}{\partial y} \tag{6.5}$$

which is simply the material derivative following the geostrophic wind.

In addition to a nearly geostrophic horizontal wind ("quasi-geostrophic"), we assume that the vertical distribution of pressure is nearly hydrostatic ("quasi-hydrostatic"). Recall that although we do not have a prognostic (forecast) equation for w, this does not mean that w is zero, but rather that it must be deduced diagnostically from the other variables. As was done in Section 2.4.3,

we assume a *reference atmosphere* (denoted here by overbars) that is at rest and in exact hydrostatic balance:

$$\frac{\partial \overline{p}}{\partial z} = -\overline{\rho} g$$

Perturbations from the reference state are also in hydrostatic balance,

$$\frac{\partial p}{\partial z} = \frac{\rho_0}{\overline{\theta}} \theta g \tag{6.6}$$

where p and θ are the disturbance pressure and potential temperature, respectively, ρ_0 is a constant density (a result of the Boussinesq approximation), and $\overline{\theta}$ is a function of z only. The full value of potential temperature will be denoted by θ_{tot}.

Together, the assumptions of geostrophic and hydrostatic balance produce the thermal wind relation (see Section 3.4):

$$\mathbf{V}_{\text{T}} = \frac{\partial \mathbf{V}_g}{\partial z} = \frac{g}{f\overline{\theta}} \mathbf{k} \times \nabla_h \theta \tag{6.7}$$

We notice that the disturbance potential temperature plays the same role as pressure does for the geostrophic wind: Wind flows along the contours with greatest magnitude near the largest gradients.

From equation (2.54), in the absence of strong diabatic heating, and for a small Rossby number, the first law of thermodynamics can be expressed as

$$\boxed{\frac{D\theta}{Dt_g} = -w \frac{d\overline{\theta}}{dz}} \tag{6.8}$$

which is the **quasi-geostrophic thermodynamic energy equation**. Equation (6.8) says that the perturbation potential temperature following the geostrophic motion changes due to vertical advection of the reference potential temperature. Note that the appearance of vertical advection in (6.8) reflects the large static stability of the reference atmosphere (on the order of $1/Ro$). To simplify the subsequent discussion, we take the static stability to be constant, which is a reasonable leading-order approximation for the troposphere. This implies that the buoyancy frequency (see Section 2.7.3),

$$N = \left[\frac{g}{\overline{\theta}} \frac{d\overline{\theta}}{dz} \right]^{1/2} \tag{6.9}$$

is also constant.

Finally, since many results that follow assume a familiarity with the gradient and Laplacian operations on scalar fields, we provide a brief review of these terms and their interpretation. Given a two-dimensional scalar function, ϕ, the gradient of ϕ, $\nabla_h \phi$, is a *vector* quantity that is directed toward larger values and

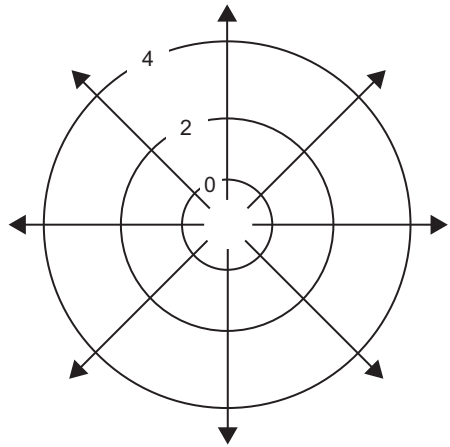

FIGURE 6.9 Illustration of the gradient operator for a scalar function, ϕ. The gradient of ϕ, a vector field, is illustrated by *arrows* that are directed toward larger values and orthogonal to *lines* of constant ϕ. The Laplacian is given by the divergence of the gradient, which is a local maximum near the local minimum in ϕ.

orthogonal to lines of constant ϕ (Figure 6.9). The Laplacian is given by the divergence of the gradient of ϕ, $\nabla_h^2\phi = \nabla_h \cdot (\nabla_h \phi)$, which is a *scalar* quantity. Since the gradient points toward larger values, the Laplacian is positive and a local maximum near local minima in ϕ; conversely, the Laplacian is negative and a local minimum near local maxima in ϕ.

6.3 POTENTIAL VORTICITY DERIVATION OF THE QG EQUATIONS

Consider now conservation of potential vorticity, which will provide the basis for one perspective of quasi-geostrophic dynamics. In Sections 5.3.2 and 5.5.2, we discovered that fast gravity-wave motions have zero potential vorticity. The dynamics of extratropical weather systems are more closely related to Rossby waves, which are geostrophically balanced and have nonzero PV, so it proves useful to filter the gravity waves from the governing equations. This is accomplished by the linearized PV equation (5.91), but the linear dynamics are deficient in many aspects needed to understand weather systems, including interactions between these systems and the jet stream. These interactions come from advection terms in the PV equation, which are lacking in (5.91) and must be reintroduced. It turns out that this is easily accomplished. First, we use the perturbation method of Section 5.1 to linearize the Ertel PV around the reference atmosphere described in Section 6.2.1, while retaining the nonlinear advection terms. Second, we replace the wind by the geostrophic wind in both the PV and the advection terms by the reasoning leading to (6.5).

For the Boussinesq approximation, the Ertel PV conservation law (4.24) can be expressed as

$$\frac{D\Pi}{Dt} = \frac{D}{Dt}\left[\frac{\boldsymbol{\omega}_a \cdot \nabla\theta_{\text{tot}}}{\rho_o}\right] = 0 \tag{6.10}$$

where

$$\boldsymbol{\omega}_a = (\eta, \xi, \zeta + f) \tag{6.11}$$

is the three-dimensional vorticity vector. Since $\nabla\theta_{\text{tot}} = \left(\frac{\partial\theta}{\partial x}, \frac{\partial\theta}{\partial y}, \frac{\partial\theta}{\partial z} + \frac{d\overline{\theta}}{dz}\right)$, we immediately notice that the x and y contributions to the dot product in (6.10) involve nonlinear terms[2] and must be discarded, leaving

$$\frac{D}{Dt}\left[\frac{1}{\rho_o}(\zeta + f)\frac{\partial\theta_{\text{tot}}}{\partial z}\right] = 0 \tag{6.12}$$

Substituting $\theta_{\text{tot}} = \overline{\theta} + \theta$, and again discarding nonlinear terms gives

$$\frac{D}{Dt}\frac{1}{\rho_o}\left[(\zeta + f)\frac{d\overline{\theta}}{dz} + f\frac{\partial\theta}{\partial z}\right] = 0 \tag{6.13}$$

Factoring the constant $\frac{d\overline{\theta}}{dz}$ yields

$$\frac{D}{Dt}\frac{1}{\rho_o}\frac{d\overline{\theta}}{dz}\left[\zeta + f + f\frac{\partial}{\partial z}\left(\frac{d\overline{\theta}}{dz}^{-1}\theta\right)\right] = 0 \tag{6.14}$$

Although $\frac{d\overline{\theta}}{dz}$ is assumed constant, we introduce it within the vertical derivative since this general form holds even in the case where $\frac{d\overline{\theta}}{dz}$ is a function of z. Finally, approximating the wind geostrophically gives

$$\frac{D}{Dt_g}\frac{1}{\rho_o}\frac{d\overline{\theta}}{dz}\left[\zeta_g + f + f\frac{\partial}{\partial z}\left(\frac{d\overline{\theta}}{dz}^{-1}\theta\right)\right] = 0 \tag{6.15}$$

or

$$\boxed{\frac{D}{Dt_g}\frac{1}{\rho_o}\frac{d\overline{\theta}}{dz}q = 0} \tag{6.16}$$

where

$$\boxed{q = \zeta_g + f + f\frac{\partial}{\partial z}\left(\frac{d\overline{\theta}}{dz}^{-1}\theta\right)} \tag{6.17}$$

is the **quasi-geostrophic potential vorticity** (QG PV).

[2]Products of the functions of the dependent variables—in this case, disturbance vorticity and potential temperature.

Equation (6.16) says that the QG PV is conserved following the geostrophic motion, analogous to Ertel PV conservation following the full flow. We note that the leading factor, $\frac{1}{\rho_o}\frac{d\overline{\theta}}{dz}$, is independent of time and merely scales the QG PV by a constant function of z. It is customary to discard this factor; however, in doing so the units change to those of vorticity (s^{-1}). Although, as a result of linearization, the QG PV involves a sum of vorticity and static stability compared to a product for the Ertel PV, the dynamical interpretation following an air parcel is qualitatively similar: Increases in vorticity must be accompanied by decreases in static stability in order to conserve PV.

Taking the vertical derivative of the quasi-geostrophic thermodynamic energy equation (6.8) and using the result to replace the static stability term in (6.15) gives

$$\boxed{\frac{D}{Dt_g}\left(\zeta_g + f\right) = f\frac{\partial w}{\partial z}} \tag{6.18}$$

which is the **quasi-geostrophic vorticity equation**. Following the geostrophic motion, the geostrophic absolute vorticity, $\zeta_g + f$, changes due to stretching of planetary rotation by vertical motion. The fact that the contribution from stretching of relative vorticity is absent indicates that the quasi-geostrophic approximation is only formally valid when the relative vorticity is small compared to f. This is consistent with the small Rossby number approximation, since the ratio of the scaling for vorticity, U/L, to f is $U/(fL)$. Fortunately, it turns out that quasi-geostrophic equations remain qualitatively useful for observed disturbance amplitudes despite this restrictive condition. The vertical motion in the quasi-geostrophic vorticity equation is linked to horizontal motion by the **quasi-geostrophic mass continuity equation**,

$$\boxed{\frac{\partial u_a}{\partial x} + \frac{\partial v_a}{\partial y} + \frac{\partial w}{\partial z} = 0} \tag{6.19}$$

where $\mathbf{V}_a = (u_a, v_a)$ is the ageostrophic wind. This result derives directly from the Boussinesq approximation (see 2.60) and the fact that the geostrophic wind is horizontally nondivergent on the f-plane.

We return now to the question of momentum conservation for the quasi-geostrophic approximation. If we approximate the momentum geostrophically in the momentum equations (e.g., 2.24 and 2.25), steady-state expressions result and there are no dynamics. Therefore, ageostrophic effects must be present in the momentum equation (hence, *quasi*-geostrophy), and this is one reason why we did not begin our analysis with momentum conservation. Approximating the material derivative geostrophically, the momentum equation can be written in general as

$$\frac{D\mathbf{V}_g}{Dt_g} = -\frac{1}{\rho_o}\nabla_h(p_g + p_a) - f\mathbf{k}\times(\mathbf{V}_g + \mathbf{V}_a) \tag{6.20}$$

which allows for ageostrophic effects in both the pressure and wind fields. Forming a vorticity equation as in Chapter 4, by taking $\frac{\partial}{\partial x}$ of the v_g-momentum equation minus $\frac{\partial}{\partial y}$ of the u_g-momentum equation, gives

$$\frac{D\zeta_g}{Dt_g} = -f\left(\frac{\partial u_a}{\partial x} + \frac{\partial v_a}{\partial y}\right) = f\frac{\partial w}{\partial z} \tag{6.21}$$

where the last equality is accomplished by the quasi-geostrophic mass continuity equation. Noting that f is a constant allows it to be added to the material derivative, which recovers the quasi-geostrophic vorticity equation (6.18). This shows that (6.20) is consistent with the previously derived equations, but for reasons described subsequently, there is ambiguity in the individual terms in (6.20).

Ambiguity in the momentum equation involves two effects. First, since the curl of a gradient is zero, we may add an arbitrary field, $\tilde{p}_a$, to p_a in (6.20) and arrive at the same vorticity equation, (6.18). Second, we may add an arbitrary vector field, $\tilde{\mathbf{V}}_a$, to the ageostrophic wind in the momentum equation and arrive at the same vorticity equation, provided that $\nabla_h \cdot \tilde{\mathbf{V}}_a = 0$. Thus, p_a and $\mathbf{V}_a$ are arbitrary fields, but they are related through the **quasi-geostrophic divergence equation**,

$$\nabla_h^2 p_a = \rho_0 f \zeta_a + 2J(u_g, v_g) \tag{6.22}$$

which is obtained from equation (6.20) by taking $\frac{\partial}{\partial x}$ of the u_g-momentum equation plus $\frac{\partial}{\partial y}$ of the v_g-momentum equation. Here, $J(u_g, v_g) = \frac{\partial u_g}{\partial x}\frac{\partial v_g}{\partial y} - \frac{\partial v_g}{\partial x}\frac{\partial u_g}{\partial y}$ is a Jacobian, and $\zeta_a = \frac{\partial v_a}{\partial x} - \frac{\partial u_a}{\partial y}$ is the ageostrophic vertical vorticity. Although (6.22) provides a diagnostic equation relating the ageostrophic pressure and the rotational part of the ageostrophic wind to the geostrophic wind, lacking additional information, one of the ageostrophic quantities must be eliminated in order to close the system. This choice is arbitrary, and therefore so are the terms on the right side of (6.20). The most common choice, $p_a = 0$, puts all ageostrophic effects into $\mathbf{V}_a$, giving the **quasi-geostrophic momentum equation**

$$\boxed{\frac{D\mathbf{V}_g}{Dt_g} = -f\mathbf{k} \times \mathbf{V}_a} \tag{6.23}$$

We emphasize that this arbitrary choice has no effect on the dynamics of vorticity or potential vorticity. The divergent part of the ageostrophic wind is well constrained through the continuity equation and will play an essential role in "w-Thinking." First we explore the "PV Thinking" view of quasi-geostrophic dynamics, which has no role for ageostrophic motion.

Section's Key Points

- The QG equations are defined by a small Rossby number and for a reference atmosphere that has strong stratification.
- The QG PV is a linearization of the Ertel PV consisting of a sum of contributions from the vertical component of vorticity and the disturbance static stability.
- Following the geostrophic motion, geostrophic vorticity changes due to stretching of ambient planetary rotation.
- Neglecting ageostrophic effects on pressure, following the geostrophic motion, geostrophic momentum changes due to Coriolis turning of the ageostrophic wind. The divergent ageostrophic wind links to vertical motion by the mass continuity equation, and the rotational ageostrophic wind is approximated from the geostrophic wind by the QG divergence equation.

6.4 POTENTIAL VORTICITY THINKING

The fact that potential vorticity conservation represents all of the fundamental physical conservation laws in a single equation provides the basis for a very powerful and simple interpretation of the dynamics of weather systems. Before reviewing the two essential elements comprising "PV Thinking," inversion and conservation, we examine the scaling properties of the QG PV.

Using the geostrophic and hydrostatic relationships to replace the vorticity and potential temperature in the QG PV (6.17), and recalling that N is the buoyancy frequency, gives

$$q - f = \frac{1}{\rho_o f}\nabla_h^2 p + \frac{1}{\rho_o}\frac{\partial}{\partial z}\frac{f}{N^2}\frac{\partial p}{\partial z} \tag{6.24}$$

so that the QG PV is determined completely by the pressure field. This remarkable fact will allow us to make forecasts knowing only the pressure at the initial time, and to understand why and how the system evolves. Nondimensionalizing (6.24) using length scales L and H in the horizontal and vertical, respectively, and a geostrophic scaling[3] for the pressure field, $p \sim \rho_o U f L$ gives

$$q - f \sim \frac{U}{L}\left(\hat{\nabla}_h^2 \hat{p} + \frac{1}{B^2}\frac{\partial^2 \hat{p}}{\partial \hat{z}^2}\right) \tag{6.25}$$

where we have assumed that the buoyancy frequency, N, is a constant, hats denote nondimensional variables that are assumed to have values on the order of one, and B is the nondimensional Burger number. In analogy with vorticity, $q - f$ may be thought of as the "relative" QG PV, and we see that the natural scaling for this quantity is the same as for vertical vorticity, U/L. Including the

[3]The nondimensional geostrophic wind is then given in terms of the nondimensional pressure by $\hat{\mathbf{V}}_g = -\hat{k} \times \hat{p}$.

scaling factor from (6.16) gives a scaling for QG PV, $\frac{U}{\rho_o L}\frac{d\overline{\theta}}{dz}$, in the same units as the Ertel PV.

The Burger number is a fundamental measure of the importance of stratification relative to rotation, and can be expressed in at least four useful forms:

$$B = \frac{NH}{fL} = \frac{L_R}{L} = \frac{H}{H_R} = \frac{Ro}{Fr} \tag{6.26}$$

The second equality shows that the Burger number is given by the ratio of the Rossby radius, $L_R = \frac{NH}{f}$, to the scaling length of the motion, L. Disturbances that are large compared to the Rossby radius have a small Burger number, which promotes the importance of vortex stretching. The third equality shows that the Burger number is also given by the ratio of the scaling depth, H, to the Rossby depth, $H_R = \frac{fL}{N}$. Rossby depth measures the vertical influence of disturbances, which increases with disturbance length scale and rotation, and for smaller static stability. Finally, the Burger number is also given by the ratio of the Rossby number, $Ro = \frac{U}{fL}$, to the Froude number, $Fr = \frac{U}{NH}$, both of which are nondimensional. As we have seen, the Rossby number measures the importance of disturbance vorticity, $\frac{U}{L}$, relative to the ambient vorticity, f, and, in the present context, the Froude number[4] measures the importance of disturbance vertical shear, $\frac{U}{H}$, relative to the buoyancy frequency, N. In deriving the QG equations we have assumed strong ambient rotation ($\zeta \ll f$) and stratification (large $\frac{d\overline{\theta}}{dz}$), so that both Ro and Fr are small (much less than one), which implies a Burger number close to unity and equal importance for the two terms in the QG PV. This in turn implies that the natural disturbance length scales are $L \sim L_R$ and $H \sim H_R$, which provide useful guides in discussing the dynamics of weather features.

Section's Key Points

- The QG PV is determined completely by the pressure field.
- The relative importance of the vorticity and static stability contributions to the QG PV is measured by the Burger number.

6.4.1 PV Inversion, Induced Flow, and Piecewise PV Inversion

PV inversion is a kinematic diagnostic technique involving the recovery of other fields from the PV. For unity B, (6.25) can be written as

$$\hat{q} - Ro^{-1} = \hat{\nabla}^2 \hat{p} \tag{6.27}$$

[4]By the thermal-wind relationship, vertical shear of the geostrophic wind is proportional to the horizontal temperature gradient, so the Froude number measures the slope of the isentropes.

The constant Ro^{-1} is due to the ambient rotation and stratification and, although large, has no dynamical significance since it merely changes the value of the PV everywhere. Therefore, features of interest in the nondimensional QG PV, $\hat{q}$, are determined by the Laplacian of the nondimensional pressure field. Areas of relatively low pressure are associated with large values of QG PV, and areas of high pressure with relatively small QG PV. QG PV inversion involves recovering the pressure from QG PV by solving

$$\hat{p} = \hat{\nabla}^{-2}\hat{q} \tag{6.28}$$

Since $\hat{\nabla}^2$ involves taking derivatives, we expect that $\hat{\nabla}^{-2}$ will involve taking antiderivatives, integrals, to recover the pressure field from the QG PV.

Returning to the full-dimensional form of the QG PV, multiplying (6.24) by f we find

$$f(q-f) = \frac{1}{\rho_o}\nabla_h^2 p + \frac{1}{\rho_o}\frac{\partial}{\partial z}\frac{f^2}{N^2}\frac{\partial p}{\partial z} = \mathsf{L}p \tag{6.29}$$

where

$$\mathsf{L} = \frac{1}{\rho_o}\nabla_h^2 + \frac{1}{\rho_o}\frac{\partial}{\partial z}\frac{f^2}{N^2}\frac{\partial}{\partial z} \tag{6.30}$$

is an operator that is approximately a three-dimensional Laplacian, "stretched" in the z direction relative to x and y by $\frac{f^2}{N^2}$; the nondimensionalized version discussed in (6.28) removes this stretching. The product fq is a useful combination because it is positive (negative) for cyclones (anticyclones) in both Northern and Southern hemispheres, providing a "hemispherically neutral" interpretation for PV Thinking.[5] Since L acts like a Laplacian, $f(q-f)$ will be a maximum where p is a minimum, which for cyclones implies $q > 0$ in the Northern Hemisphere and $q < 0$ in the Southern Hemisphere; the reverse applies to anticyclones.

As for the nondimensional case, symbolically we may define QG PV inversion by the operator that reverses the action of L,

$$p = \mathsf{L}^{-1}(fq) \tag{6.31}$$

which recovers the pressure field from the QG PV field (the constant from $L^{-1}f^2$ is taken to be zero). Given the pressure field, the geostrophic wind and the disturbance potential temperature are recovered from (6.1) and (6.6), respectively. From this point of view, the wind and potential temperature field are "induced," or caused, by the QG PV.

[5]This relation derives from relative vorticity, so that cyclones have the same sign as the local planetary rotation, f.

Boundary conditions must be supplied when inverting the potential vorticity. Assuming periodic conditions in the horizontal, boundary conditions on horizontal boundaries such as the surface include a specification of the pressure (Dirichlet condition), the vertical derivative of pressure (Neumann condition), or a linear combination of the pressure and its vertical derivative (Robin condition); "free-space" solutions apply in the absence of boundary conditions. From the hydrostatic equation (6.6), Neumann conditions involve a specification of the potential temperature field at the boundary. Assuming that the surface potential temperature field is independent of the potential vorticity provides a powerful approach to atmospheric dynamics because both the QG PV and θ are conserved following the motion. Since the conservation law for surface potential temperature (6.8 with $w = 0$) resembles that for QG PV (6.16), surface potential temperature may be thought of as QG PV at the surface. Mathematically, one can make this association precise by replacing the inhomogeneous Neumann boundary condition with a homogeneous one (setting $\theta = 0$ at $z = 0$), provided the QG PV is augmented by a "spike" contribution at $z = 0$ that is directly proportional to surface θ. This "PV-θ" perspective is particularly useful for understanding how PV anomalies in the troposphere, such as those associated with tropopause undulations, interact with surface features, such as surface cyclones.

To illustrate the concepts associated with PV inversion, we consider two canonical disturbances in this chapter. The first disturbance is modeled after a "short-wave" trough, which appears on upper-tropospheric weather maps as an isolated trough of low pressure (low geopotential height on pressure surfaces). This disturbance is associated with a localized blob of cyclonic QG PV, taken here to be in the middle troposphere with Gaussian structure and a maximum value of 2 PVU (Figure 6.10). The flow induced by the PV blob is largest near the "edge" of the disturbance, and decays with distance (Figure 6.10a), which illustrates the important nonlocal aspect of the inversion: The wind is nonzero more than 1000 km from the region having QG PV. This leads to the notion of "action at a distance," where a dynamical process may depend on the flow induced by a remote PV anomaly.

The disturbance in Figure 6.10 is embedded within the simplest possible jet stream, with a zonal wind that is constant in x and y and if the zonal wind increases linearly upward from zero at the ground. Despite its simplicity, it is apparent from Figure 6.10b that this configuration is a rather good model for a short-wave trough in a westerly jet stream. The "stretched"-Laplacian solution is evident in the vertical cross-sections, which reveal that the nonlocal influence extends to the surface, with an area of low pressure due to the QG PV aloft (Figure 6.10c). Finally, in Figure 6.10d we see that the PV blob is associated with a local maximum in cyclonic vorticity, cyclonic wind flow around the PV blob, and a local maximum in static stability, with "warm" air above the PV blob and "cold" air below.

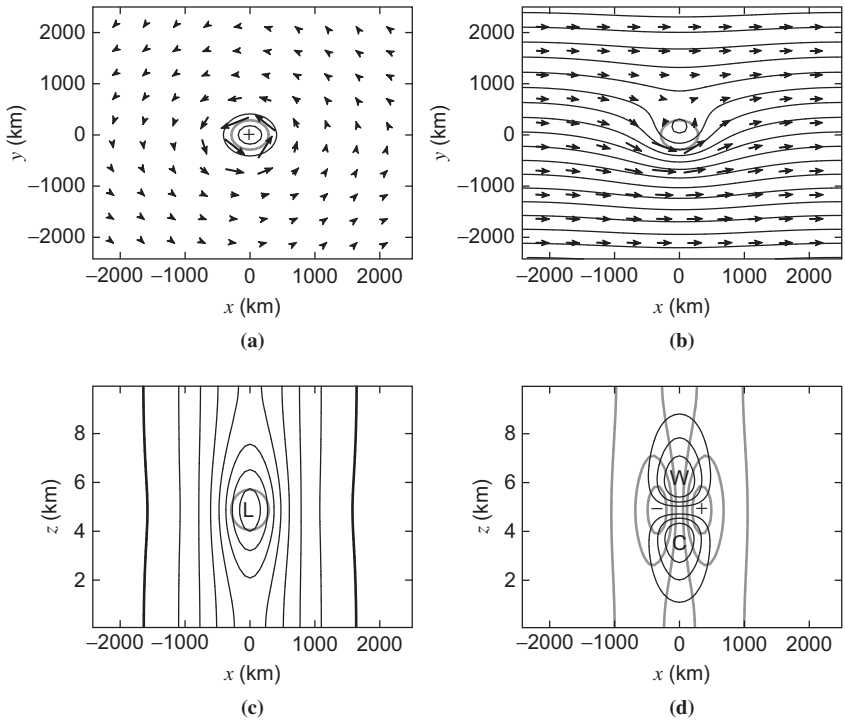

FIGURE 6.10 Inversion of an idealized localized blob of QG PV having a magnitude of 2 PVU embedded in a jet stream consisting of a westerly wind increasing linearly with height. (a) PV contours at altitude of 5 km are shown every 0.5 PVU; wind induced by the PV anomaly is shown by *arrows*, with a maximum wind speed of 22 m s^{-1}; (b) *pressure contours* every 42 hPa (equivalent to 60-m height contours on an isobaric surface) and full wind vectors (wind due to the PV anomaly plus the westerly jet), with a maximum wind speed of 36 m s^{-1}; (c) anomaly pressure every 21 hPa (equivalent to 30-m height contours) with *bold zero contour*; and (d) meridional wind every 6 m s^{-1} and potential-temperature anomalies every 2 K ("W" and "C" imply "warm" and "cold" values). In (a) through (c), the 1-PVU QG PV contour is denoted by the *thick gray line*.

As mentioned previously, surface potential temperature plays the role of PV. Warm (cold) air at the surface is associated with low (high) pressure and, by thermal wind reasoning, cyclonic circulation that decays upward from the surface into the troposphere (Figure 6.11). This may be understood from the hydrostatic equation and the fact that, with zero QG PV, solutions to Laplace problems have extrema on the boundaries. A leading-order approximation to the tropopause is a rigid boundary similar to the surface, in which case cold (warm) air is associated with low (high) pressure and cyclonic (anticyclonic) circulation that decays downward from the tropopause.

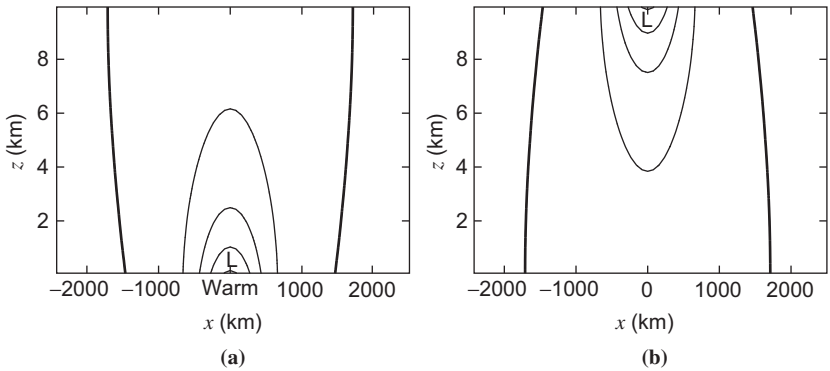

FIGURE 6.11 Pressure contours associated with (a) surface warm anomaly and (b) tropopause cold anomaly. Pressure is contoured every 21 hPa (equivalent to 30-m height contours) with *bold zero contour*. The potential temperature anomalies have an amplitude of 10 K and the same horizontal shape as the PV anomaly in Figure 6.10.

The notion of induced flow is most powerful when considering discrete portions of the atmosphere, and their interaction (i.e., dynamics). Since the QG PV operator, L, is linear, the atmosphere may be broken into components, the sum of which gives the full fields. This "piecewise PV inversion" framework is expressed mathematically as

$$p = \sum_{i=1}^{N} p_i = \sum_{i=1}^{N} \mathrm{L}^{-1}(fq_i) \tag{6.32}$$

To each PV element, q_i, one associates a pressure field, p_i, from which the wind and temperature may be recovered; adding up the pieces gives the full field for each variable (because geostrophic and hydrostatic balance are also linear operations).

To illustrate the concept of piecewise PV inversion we introduce the second canonical disturbance: a straight localized wind maximum within the westerly jet stream known as a "jet streak" (Figure 6.12). An elliptical dipole is used to model the jet streak, with a cyclonic QG PV anomaly poleward of an anticyclonic QG PV anomaly. The flow induced by this dipole produces a jet of strong wind between them (Figure 6.12a) and, adding in the simple linear westerly jet as in the previous example, we see a spatially localized burst of stronger wind within the broader westerlies (Figure 6.12b). Considering now the flow induced by only the positive and negative ellipses of QG PV, we see that the jet is present between the vortices because the contribution from each ellipse reinforces that from the other in this location. Moreover, the flow from each ellipse extends to the other vortex in a symmetrical fashion (Figure 6.12c, d). The dynamics of this system are simply understood by the component of flow from each ellipse

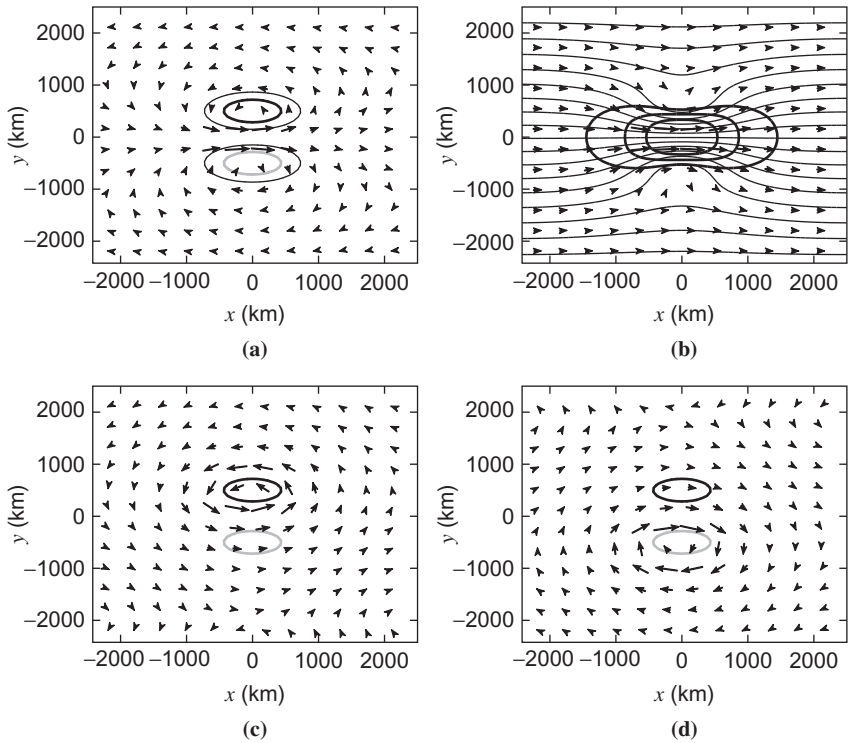

FIGURE 6.12 Idealized model of a "jet streak" as a dipole of QG PV having a magnitude of 2 PVU embedded in a jet stream consisting of a westerly wind increasing linearly with height. (a) PV contours at a height of 5 km are shown every 0.5 PVU; wind induced by the PV anomaly is shown by *arrows*, with a maximum wind speed of 22 m s^{-1}; (b) pressure contours at 5 km every 42 hPa (equivalent to 60-m geopotential height contours on an isobaric surface), full wind vectors (wind due to the PV dipole plus the westerly jet), and isotachs (20, 30, and 40 m s^{-1}) in *thick lines*; (c) wind induced by the positive anomaly; (d) wind induced by the negative PV anomaly. In (c) and (d) the −1- and 1-PVU QG PV contours are denoted by the *thick* gray and black lines, respectively.

advecting the QG PV, which reveals that (1) there is very little dynamics associated with each ellipses' "self" advection; and (2) the dynamics focus around the advection of the QG PV by the opposing ellipse, which advects the ellipses symmetrically downstream (the system moves in a straight line) at a speed much slower than the wind in the jet streak itself.

Section's Key Points

- The pressure field is determined completely by the QG PV through an inversion relationship. Through the geostrophic and hydrostatic relations, the

geostrophic wind and potential temperature fields are recovered from the QG PV as well.
- Warm air at the surface is analogous to cyclonic QG PV; cold air at the tropopause is analogous to cyclonic QG PV.
- QG PV inversion is defined by a Laplacian-like operator, so that local maxima in cyclonic QG PV yield local minima in pressure.
- Piecewise QG PV inversion involves breaking the QG PV field into components and associating with each component a pressure field by QG PV inversion; the sum of the pieces is equal to the total pressure field.

6.4.2 PV Conservation and the QG "Height Tendency" Equation

Given the ability to recover the geostrophic wind from the QG PV, QG prediction may now be explored from the PV Thinking perspective. Expanding the QG material derivative in (6.16) gives

$$\frac{\partial q}{\partial t} = -\mathbf{V}_g \cdot \nabla_h q \tag{6.33}$$

which says that the time rate of change of QG PV at a point in space is determined entirely by the advection of the QG PV by the geostrophic wind. This provides the basis for a dynamical forecast model. Given an initial distribution of QG PV, one inverts this field for the pressure using (6.31), which then gives the geostrophic wind. Knowledge of the QG PV and geostrophic wind allows for a prediction of the future configuration of the QG PV from (6.33). At the future time, the QG PV can be inverted for the wind, and the process repeated indefinitely into the future.

To complete the picture, however, we need to specify boundary conditions for (6.33). At Earth's surface, which we approximate as a rigid horizontal surface, there is no vertical motion, and therefore the QG thermodynamic energy equation takes the form

$$\frac{\partial \theta}{\partial t} = -\mathbf{V}_g \cdot \nabla_h \theta \tag{6.34}$$

Notice that this equation is identical to (6.33), where θ plays the role of q. Therefore, in addition to advancing q by (6.33), we also advance θ by (6.34), which provides boundary conditions for the QG PV inversion at the future time. For the upper boundary condition, another rigid horizontal boundary may be used to represent either a crude approximation to the tropopause or a higher level in the stratosphere.

This approach is an extremely powerful approximation to the evolution of extratropical weather systems, where one needs to evaluate the horizontal advection of only a single quantity to predict the future, compared to solving complicated equations for five variables in the full system (u, v, w, p, θ).

Nevertheless, we do not measure QG PV directly, and a forecast of pressure is often more intuitive. We may obtain a pressure forecast equation from (6.33) by noting that $\frac{\partial}{\partial t} f(q-f) = \frac{\partial}{\partial t}(fq) = \mathsf{L}\frac{\partial p}{\partial t}$, so that

$$\mathsf{L}\frac{\partial p}{\partial t} = -\mathbf{V}_g \cdot \nabla_h (fq) \tag{6.35}$$

Here, L is the quasi-Laplacian operator (6.30). Therefore, in order to obtain the pressure tendency, $\frac{\partial p}{\partial t}$, we apply the inversion operator L^{-1} to the QG PV advection term. We expect that near local maxima in QG PV advection, such as downwind of a QG PV maximum, the pressure tendency will be a local minimum (that is, the pressure will fall).

Boundary conditions for the pressure tendency are obtained using the hydrostatic equation (6.6) in (6.34) to yield

$$\frac{\partial}{\partial z}\frac{\partial p}{\partial t} = \frac{\rho_0 g}{\bar{\theta}}\left(-\mathbf{V}_g \cdot \nabla_h \theta\right) \tag{6.36}$$

Warm-air advection at the surface implies that the pressure tendency increases upward from the surface so that, if the tendency is negative (pressure falls), it will be most negative on the boundary.

Replacing q on the right side of (6.35) using (6.17) gives

$$\mathsf{L}\frac{\partial p}{\partial t} = -\mathbf{V}_g \cdot \nabla_h \zeta_g - \mathbf{V}_g \cdot \nabla_h \left(f \frac{\partial}{\partial z} \frac{d\bar{\theta}}{dz}^{-1} \theta \right) \tag{6.37}$$

Using the thermal-wind equation (6.7) on the last term leaves

$$\boxed{\mathsf{L}\frac{\partial p}{\partial t} = -\mathbf{V}_g \cdot \nabla_h (f\zeta_g) + f^2 \frac{\partial}{\partial z}\left[\frac{d\bar{\theta}}{dz}^{-1}\left(-\mathbf{V}_g \cdot \nabla_h \theta\right)\right]} \tag{6.38}$$

which is known as the **quasi-geostrophic pressure tendency equation**, or the **height tendency equation** since, in pressure coordinates, geopotential height plays the role of pressure (see Section 6.7). Recalling the rough rule of thumb that L reverses the sign of the quantity it operates upon, we see that pressure will decrease in time where there is (1) cyclonic geostrophic vorticity advection by the geostrophic wind, and (2) an upward increase in the geostrophic advection of potential temperature. An example of the first situation occurs downwind of upper-level troughs, since cyclonic vorticity is a local maximum in troughs. An example of the second situation occurs where cold air advection in the lower troposphere decreases with height, such as behind a surface cold front. Notice that if the atmosphere is very stable $\left(\text{large } \frac{d\bar{\theta}}{dz}\right)$, the pressure tendency is dominated by vorticity advection *and*, from (6.30), the response is local in the vertical, so that the dynamics become a set of nearly horizontal uncoupled layers.

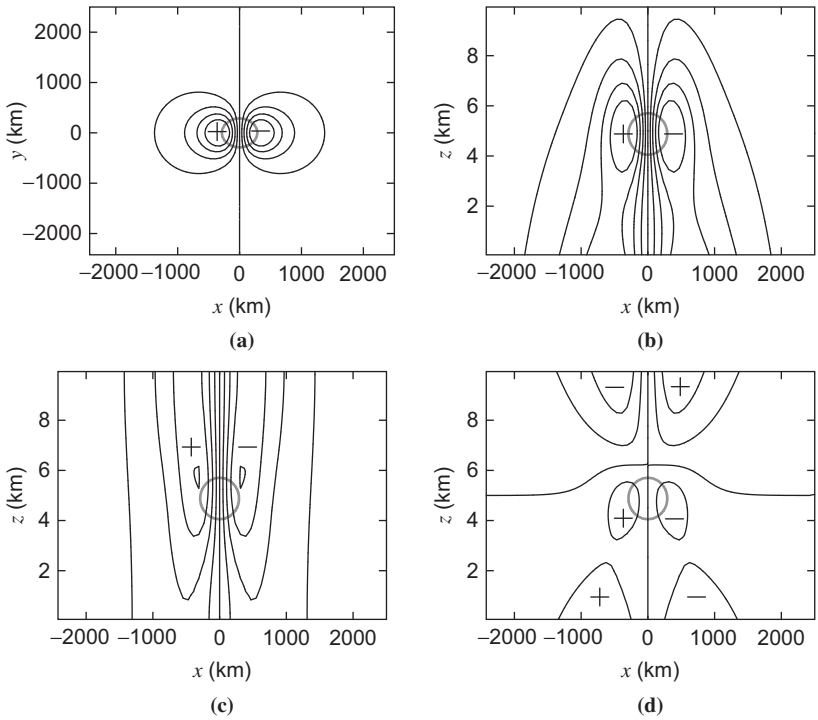

FIGURE 6.13 Pressure tendency associated with the PV blob in vertical shear shown in Figure 6.10. Pressure tendency: (a) plan view at 5-km altitude; (b) cross-section along $y = 0$; (c) cross-section along $y = 0$ of vorticity advection contribution; and (d) cross-section along $y = 0$ of temperature advection contribution. The sum of (c) and (d) equals (b). Pressure tendency *contours* are shown every 5 hPa (day)$^{-1}$, and the 1-PVU QG PV contour by a *thick gray line*.

For the PV blob in westerly shear (refer to Figure 6.10), solution of the pressure tendency equation shows, as expected, that the pressure falls downwind of the PV blob (Figure 6.13a). In the vertical, the pressure falls over a deep layer downwind of the upper-level feature, including at the surface (Figure 6.13b). The response is asymmetric in the vertical direction due to the boundary condition (6.36): Warm air advection to the right of the PV blob implies an upward increase in $\frac{\partial p}{\partial t}$ at the boundaries, so that pressure falls are a local minimum at the surface. From the PV perspective, recall that warm air on the surface acts like cyclonic QG PV, whereas warm air on the tropopause acts like anticyclonic PV; therefore, temperature advection on the surface reinforces the tendency from the PV blob, whereas there is cancellation on the tropopause.

Examining the individual contributions from advection of vorticity and potential temperature, we see that, due to the increase of westerly winds with height, the magnitude of the pressure tendency from vorticity advection is

largest above the PV blob and the pressure tendency from potential temperature advection changes sign between the surface and tropopause (Figure 6.13c, d) due in part to the boundary condition effect described previously.

Section's Key Points

- Pressure falls near local maxima of cyclonic QG PV advection.
- Pressure falls near local maxima of cyclonic geostrophic vorticity PV advection.
- Pressure falls near locations having an increase with height of the geostrophic advection of potential temperature (cold-air advection decreasing with height or warm-air advection increasing with height).
- At the surface, geostrophic advection of potential temperature determines the sign of the vertical gradient of the pressure tendency (warm-air advection implies the pressure tendency increases with height).

6.5 VERTICAL MOTION (*w*) THINKING

Vertical motion plays no role in PV Thinking because advection of potential vorticity is determined entirely by the geostrophic wind. Although temperature and momentum adjustments are implicit in the material conservation of QG PV, it is often helpful for understanding the dynamics of weather systems to consider these changes explicitly. In this framework the QG dynamics are expressed through the thermodynamic energy and vorticity equations

$$\frac{\partial \theta}{\partial t} = -\mathbf{V}_g \cdot \nabla_h \theta - w \frac{d\overline{\theta}}{dz} \tag{6.39}$$

and

$$\frac{\partial}{\partial t}\left(\zeta_g + f\right) = -\mathbf{V}_g \cdot \nabla_h (\zeta + f) + f \frac{\partial w}{\partial z} \tag{6.40}$$

respectively. Vertical motion controls the evolution of both θ and ζ_g. Therefore, we need an equation for w, which will not only mathematically close this framework but will also provide useful information on locations where clouds might form and conditional instability might be released.

To obtain the w equation we eliminate the time derivative between (6.39) and (6.40). First, we use (6.2) and (6.6) to express vorticity and potential temperature in terms of pressure:

$$\frac{\partial \theta}{\partial t} = \frac{\overline{\theta}}{\rho_0 g} \frac{\partial}{\partial z} \frac{\partial p}{\partial t} \quad \frac{\partial \zeta}{\partial t} = \frac{1}{\rho_0 f} \nabla_h^2 \frac{\partial p}{\partial t} \tag{6.41}$$

Time tendencies of pressure can then be eliminated by taking $\frac{g}{f\overline{\theta}}\nabla^2\frac{\partial\theta}{\partial t}$ and $\frac{\partial}{\partial z}\frac{\partial\zeta}{\partial t}$, and subtracting the resulting equations, which gives

$$\nabla_h^2 w + \frac{f^2}{N^2}\frac{\partial^2 w}{\partial z^2} = \frac{g}{\overline{\theta}N^2}\nabla_h^2\left(-\mathbf{V}_g\cdot\nabla_h\theta\right) - \frac{f}{N^2}\frac{\partial}{\partial z}\left(-\mathbf{V}_g\cdot\nabla_h\zeta\right) \tag{6.42}$$

This equation is more commonly known as the "traditional form" of the **quasi-geostrophic vertical motion** equation (or "omega" equation, where omega (ω) is the symbol for vertical motion in pressure coordinates). The left side involves again a quasi-Laplacian operator,

$$\tilde{\mathsf{L}} = \nabla_h^2 + \frac{f^2}{N^2}\frac{\partial^2}{\partial z^2} \tag{6.43}$$

and its interpretation is similar to that for L in QG PV inversion (6.30). Specifically, we see that, for a given forcing, the response in w will be mainly in the horizontal when $\frac{f^2}{N^2}$ is small—that is, for small planetary rotation and large static stability.

From (6.42) we see that upward motion ($w > 0$) is associated with local maxima in warm-air advection and an upward increase in the advection of geostrophic vorticity by the geostrophic wind. In both cases, the term on the right side of (6.42) is negative, which becomes positive when we "flip the sign" for the quasi-Laplacian, $\tilde{\mathsf{L}}$.

A problem with the traditional form of the omega equation is that there exists significant cancellation between the two right-side terms. To expose this cancellation and develop two different forms of the omega equation, we need to expand the right side of (6.42). This involves taking the gradient of vector products, for which vector notation is not well suited. Just as we use vector notation to simplify mathematical manipulations when scalar notation becomes cumbersome, it is often prudent to move to *indicial notation* for situations where vector notation becomes awkward. In many ways, indicial notation is simpler and less ambiguous than vector notation; we introduce only the basic elements needed here.

Indicial notation uses a subscript index to represent the components of a vector. For example, the vector wind $\mathbf{U} = (u, v, w)$ in vector notation may be written as u_i, where $u_1 = u$, $u_2 = v$, and $u_3 = w$ in indicial notation. Similarly, the vector coordinate directions (x, y, z) may be written simply as x_i. The key simplification of indicial notation is that *repeated indices represent sums.* For example, $a_i b_i = a_1 b_1 + a_2 b_2$ in two dimensions. Indices left over after summation, called dummy indices, are free to be changed if done so consistently. The dot product between two vectors can in general be written as

$$c = \mathbf{a}\cdot\mathbf{b} = a_i\, b_j \delta_{ij} = a_i\, b_i = a_j\, b_j \tag{6.44}$$

where δ_{ij} is the Kronecker delta, which takes the value one when $i = j$ and zero otherwise, leaving the familiar sum of products of vector components. Therefore, when expressing dot products it is convenient to match the subscripts of

the effected quantities, which obviates the need for δ_{ij}. The gradient operator, ∇ in vector notation, takes the form $e_i \frac{\partial}{\partial x_i}$ for indicial notation, where e_i is a unit vector. This turns out to be useful for our purposes because all of the traditional rules of differential calculus, such as the product and chain rules, apply as usual. Advection combines the gradient operator and dot product, and appears for indicial notation as, for example,

$$U \cdot \nabla \theta = u_i \frac{\partial \theta}{\partial x_i} \tag{6.45}$$

We may now write the traditional form of the omega equation using indicial notation as

$$\tilde{\mathrm{L}} w = \frac{g}{\overline{\theta} N^2} \frac{\partial}{\partial x_i} \frac{\partial}{\partial x_i} \left(-v_j \frac{\partial \theta}{\partial x_j} \right) - \frac{f}{N^2} \frac{\partial}{\partial x_3} \left(-v_j \frac{\partial \zeta}{\partial x_j} \right) \tag{6.46}$$

where we have dropped the subscript g on the wind and vorticity, and indices i and j take values 1 and 2 (x and y directions). Taking the innermost derivatives gives

$$\begin{aligned} \tilde{\mathrm{L}} w = & \frac{g}{\overline{\theta} N^2} \frac{\partial}{\partial x_i} \left(-\frac{\partial v_j}{\partial x_i} \frac{\partial \theta}{\partial x_j} - v_j \frac{\partial^2 \theta}{\partial x_i \partial x_j} \right) \\ & - \frac{f}{N^2} \left(-\frac{\partial v_j}{\partial x_3} \frac{\partial \zeta}{\partial x_j} - v_j \frac{\partial}{\partial_j} \frac{\partial \zeta}{\partial x_3} \right) \end{aligned} \tag{6.47}$$

From the definition of vorticity, $\zeta_g = \frac{1}{\rho_o f} \frac{\partial^2 p}{\partial x_i^2}$, and the hydrostatic balance, $\frac{1}{\rho_o} \frac{\partial p}{\partial x_3} = \frac{g}{\overline{\theta}} \theta$, we find $\frac{\partial \zeta}{\partial x_3} = \frac{g}{f \overline{\theta}} \frac{\partial^2 \theta}{\partial x_i^2}$. Using this identity in (6.47), and taking the remaining derivative on the first term, gives

$$\begin{aligned} \tilde{\mathrm{L}} w = & \frac{g}{\overline{\theta} N^2} \left(-\frac{\partial^2 v_j}{\partial x_i^2} \frac{\partial \theta}{\partial x_j} - 2 \frac{\partial v_j}{\partial x_i} \frac{\partial^2 \theta}{\partial x_i \partial x_j} - v_j \frac{\partial}{\partial x_j} \frac{\partial^2 \theta}{\partial x_i^2} \right) \\ & + \frac{f}{N^2} \left(\frac{\partial v_j}{\partial x_3} \frac{\partial \zeta}{\partial x_j} + v_j \frac{\partial}{\partial x_j} \frac{g}{f \overline{\theta}} \frac{\partial^2 \theta}{\partial x_i^2} \right) \end{aligned} \tag{6.48}$$

Cancellation is now apparent between the last term of each bracketed quantity. Moreover, it may be shown that (see Problem 6.3)

$$\frac{g}{\overline{\theta} N^2} \frac{\partial^2 v_j}{\partial x_i^2} \frac{\partial \theta}{\partial x_j} = \frac{f}{N^2} \frac{\partial v_j}{\partial x_3} \frac{\partial \zeta}{\partial x_j} \tag{6.49}$$

Two other forms of the omega equation are now immediately recovered. Using (6.49) to replace the term involving vorticity in (6.48) gives the compact form

$$\tilde{\mathrm{L}} w = -2 \frac{g}{N^2 \overline{\theta}} \frac{\partial}{\partial x_i} \left(\frac{\partial v_j}{\partial x_i} \frac{\partial \theta}{\partial x_j} \right) \tag{6.50}$$

In vector notation this may be written as

$$\boxed{\tilde{\mathrm{L}}w = 2\nabla_h \cdot \mathbf{Q}} \tag{6.51}$$

where $\mathbf{Q} \equiv -\frac{g}{N^2\overline{\theta}} \frac{\partial v_j}{\partial x_i} \frac{\partial \theta}{\partial x_j}$ is the "**Q**-vector." Writing the **Q**-vector in component form,

$$\begin{aligned} \mathbf{Q} &= -\frac{g}{N^2\overline{\theta}}(Q_1, Q_2) \\ &= -\frac{g}{N^2\overline{\theta}}\left(\frac{\partial u_g}{\partial x}\frac{\partial \theta}{\partial x} + \frac{\partial v_g}{\partial x}\frac{\partial \theta}{\partial y}, \frac{\partial u_g}{\partial y}\frac{\partial \theta}{\partial x} + \frac{\partial v_g}{\partial y}\frac{\partial \theta}{\partial y}\right) \end{aligned} \tag{6.52}$$

we see that vertical motion is associated with products of horizontal wind gradients and horizontal potential temperature gradients. These effects involve changes in horizontal potential temperature gradients, which we shall explore more thoroughly in Chapter 9. Rising air is found in regions where the **Q**-vector converges, so that the righthand side of (6.51) is negative, and $\tilde{\mathrm{L}}$ flips the sign.

The direction and magnitude of the **Q**-vector at a given point on a weather map can be estimated as follows. First note that the **Q**-vector can be written as

$$\mathbf{Q} = -\frac{g}{N^2\overline{\theta}}\left(\frac{\partial \mathbf{V}_g}{\partial x}\cdot\nabla_h\theta, \frac{\partial \mathbf{V}_g}{\partial y}\cdot\nabla_h\theta\right) \tag{6.53}$$

By referring the motion to a Cartesian coordinate system in which the x axis is parallel to the local isotherm with cold air on the left, (6.53) can be simplified to give

$$\mathbf{Q} = -\frac{g}{N^2\overline{\theta}}\left|\frac{\partial \theta}{\partial y}\right| \mathbf{k} \times \frac{\partial \mathbf{V}_g}{\partial x} \tag{6.54}$$

where we have used the fact that $\partial u_g/\partial x = -\partial v_g/\partial y$ and $\frac{\partial \theta}{\partial y} < 0$ in the specified coordinates. Thus, the **Q**-vector can be obtained by evaluating the vectorial change of $\mathbf{V}_g$ along the isotherm (with cold air on the left), rotating this change vector by 90° clockwise, and multiplying the resulting vector by $\frac{g}{N^2\overline{\theta}}|\frac{\partial \theta}{\partial y}|$. An example is shown in Figure 6.14, which shows an idealized pattern of cyclones and anticyclones in a slightly perturbed westerly thermal wind. Near the center of the low, the geostrophic wind change moving eastward along the isotherm is from northerly to southerly. Thus the geostrophic wind change vector points northward, and a 90° clockwise rotation produces a **Q**-vector parallel to the thermal wind. In the highs, by the same reasoning, the **Q**-vectors are antiparallel to the thermal wind. The pattern of $\nabla \cdot \mathbf{Q}$ thus yields descent in the region of cold-air advection west of the trough, and ascent in the warm-air advection region east of the trough.

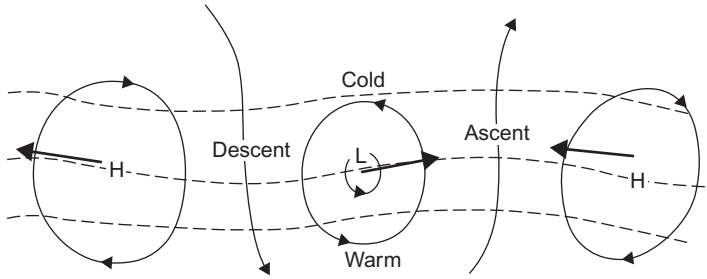

FIGURE 6.14 **Q** vectors (*bold arrows*) for an idealized pattern of isobars (*solid lines*) and isotherms (*dashed lines*) for a family of cyclones and anticyclones. (*After Sanders and Hoskins, 1990.*)

Yet another form of the omega equation is obtained using (6.49) to replace the first term in (6.48) to yield

$$\boxed{\tilde{\mathrm{L}}w = 2\frac{f}{N^2}\frac{\partial v_i}{\partial x_3}\frac{\partial \zeta}{\partial x_i} + D} \tag{6.55}$$

where $D = -2\frac{g}{\bar{\theta}N^2}\frac{\partial v_j}{\partial x_i}\frac{\partial^2 \theta}{\partial x_i \partial x_j}$ is the "deformation term." Noting that $\partial v_i\, \partial x_3$ is the thermal wind, V_T, then (6.55) becomes, in vector notation, the deformation term is one of two terms in the divergence of the **Q**-vector. In vector notation,

$$\tilde{\mathrm{L}}w = -\frac{2}{N^2}\left[-\mathbf{V}_\mathrm{T} \cdot \nabla_h (f\zeta_g)\right] + D \tag{6.56}$$

is called the *Sutcliffe form* of the QG omega equation. Neglecting the deformation term, we see that rising air is located near regions of cyclonic vorticity advection by the thermal wind. Although this approximation neglects a potentially important source of vertical motion from the deformation term, advection of vorticity by the thermal wind is easily visualized on upper-level weather maps.

The vertical motion field for the PV blob in westerly shear is shown in Figure 6.15. Notice that **Q**-vectors converge (diverge) in the region of rising (sinking) motion downwind (upwind) of the PV blob. An east–west cross-section through the PV-blob reveals the ageostrophic circulation that links rising and sinking motion by mass continuity. Consider the local time tendency of potential temperature at the level of maximum QG PV. Since disturbance potential temperature is zero at this level, there is no advection of this quantity (see Figure 6.10d), whereas the disturbance advection of the basic-state potential temperature gradient (linear decrease with y) implies increasing (decreasing) values to the right (left) of the PV blob. Geostrophic and hydrostatic balance are "disrupted" by this geostrophic advection pattern, but they are "restored" by the ageostrophic circulation. Notice that the vertical motion pattern cools

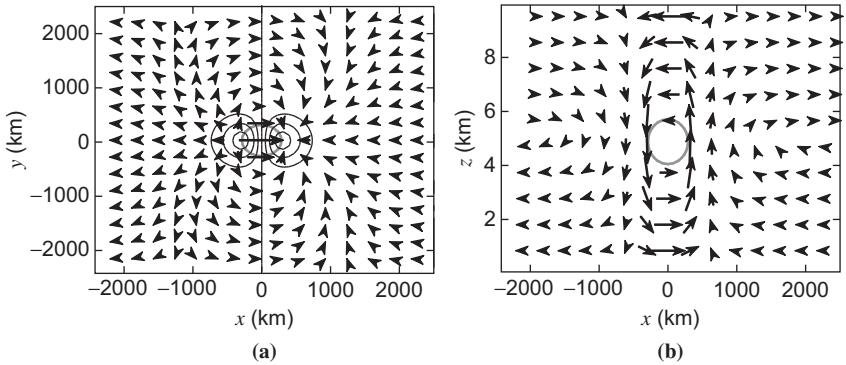

FIGURE 6.15 Vertical motion associated with the PV blob in vertical shear shown in Figure 6.10. (a) Q-vectors and contours of w every 2 cm s^{-1}, with rising air where Q-vectors converge; (b) vertical cross-section along $y = 0$ of the ageostrophic circulation (u_a, w). The 1-PVU QG PV contour is shown by a *thick gray line*.

(warms) the atmosphere in the region of rising (sinking) motion, which opposes the tendency from geostrophic advection discussed previously. Moreover, Coriolis turning of the horizontal ageostrophic wind acts to increase (decrease) the v_g component of the wind above (below) the PV blob, which restores thermal wind balance with the new potential temperature distribution. In the quasi-geostrophic equations, this adjustment "process" is instantaneous, so that the atmosphere is always in quasi-geostrophic and quasi-hydrostatic balance. Linking back to the PV view of dynamics, one can say that the ageostrophic circulations that maintain geostrophic and hydrostatic balance are required if the QG PV is to be conserved following the geostrophic motion.

Note that, in the absence of **Q**-vectors, one may still easily estimate the vertical motion pattern using the Sutcliffe form of the QG omega equation. The thermal wind, dominated by the westerly shear jet, points mostly toward positive x, so that the advection of geostrophic vorticity by the thermal wind is positive (negative) to the right (left) of the PV blob. As a result, one expects rising (sinking) motion to the right (left) of the blob. This technique can be extremely useful for quickly estimating regions of rising and sinking air from weather maps.

For the jet streak example, a four-cell pattern of vertical motion is apparent, with rising motion in the "right entrance" and "left exit" regions of the jet (Figure 6.16). Vertical cross sections through the jet entrance (Figure 6.17, left panel) and exit (Figure 6.17b) regions reveal transverse (across flow) ageostrophic circulations, which increase (decrease) zonal momentum in upper levels. These circulation patterns accelerate (decelerate) the wind into (out of) the jet, as well as increasing (decreasing) the vertical shear of the zonal wind in the jet entrance (exit) regions. Notice that, in the jet entrance region, relatively

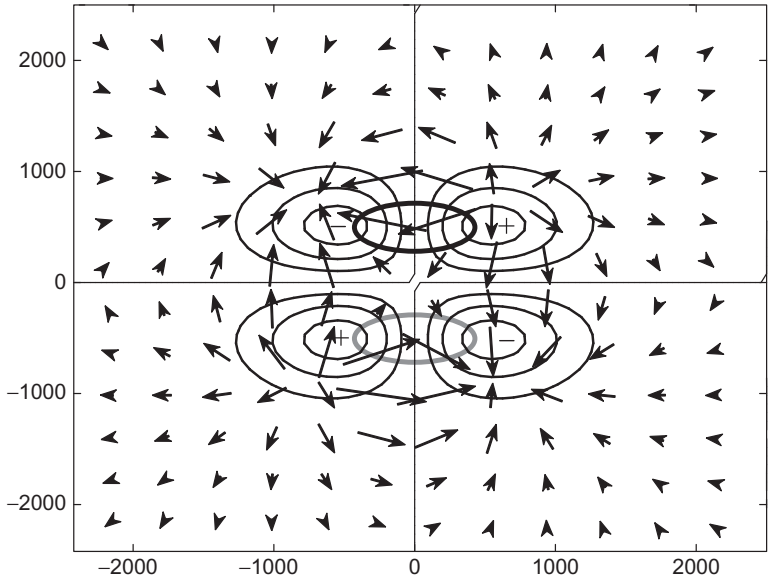

FIGURE 6.16 Vertical motion associated with the jet streak shown in Figure 6.12. *Contours* show vertical motion (w) at 5-km altitude every 1 cm s^{-1}, and *arrows* show the divergent ageostrophic wind. The −1- and 1-PVU QG PV contours are denoted by the *thick gray* and *black lines*, respectively.

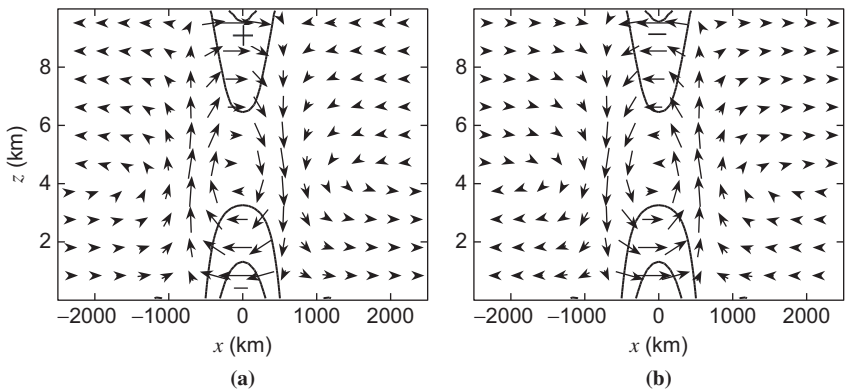

FIGURE 6.17 Vertical cross-section of ageostrophic circulation (u_a, w) near the (a) jet entrance ($x = -700$ km) and (b) jet exit ($x = 700$ km) regions. *Contours* show the acceleration of the geostrophic zonal wind, $\frac{Du}{Dt}$, every 5 m s^{-1} per hour.

warm air rises while relatively cold air sinks, which converts potential energy to kinetic energy of the stronger winds in the jet streak; the reverse process occurs in the jet exit region.

Section's Key Points

- The QG equations have a diagnostic equation for vertical motion.
- Air rises near local maxima in warm-air advection and an upward increase in the advection of geostrophic vorticity by the geostrophic wind.
- Air rises near local maxima of **Q**-vector convergence.
- Air rises near local maxima of cyclonic vorticity advection by the thermal wind.

6.6 IDEALIZED MODEL OF A BAROCLINIC DISTURBANCE

We have developed two dynamically consistent frameworks for interpreting quasi-geostrophic dynamics. Here we apply these frameworks to understand intensifying extratropical cyclones, which is a process referred to as cyclogenesis (see Figures 6.7, 6.8, and accompanying text). Figure 6.18 illustrates the main elements involved in the development process. Nearly all developing cyclones are preceded by an upper-level disturbance that is due to a downward undulation of the tropopause. This downward undulation is associated with a blob of anomalous cyclonic PV, represented by the "**+**" sign in Figure 6.18. As discussed in connection with Figure 6.10, such a PV blob is associated with low-pressure, cyclonic winds, and warm (cold) air above (below) the blob. At the surface, a developing cyclone appears downshear of the PV blob as a region of relatively warm air at the surface. As discussed in connection with Figure 6.11, anomalously warm air at the surface behaves like cyclonic PV and is associated with low pressure and cyclonic winds that weaken upward. Taken together, these PV anomalies yield pressure fields that tilt westward with height and potential temperature fields that tilt eastward with height. A final important ingredient is the ambient flow, which takes the form of westerly winds that increase upward to a maximum at the tropopause.

From the PV-θ (kinematic) perspective, low pressure develops east of the upper-level PV blob because the induced flow from the blob acts to increase the amplitude of the surface warm anomaly through warm air advection (Figure 6.18b, *heavy dashed line*). Note that this mechanism requires a poleward decrease in the ambient potential temperature field and, by thermal wind, an upward increase in westerly winds as assumed before. Similarly, given a poleward increase of PV at the level of the upper-level PV blob, the amplitude of the anomaly will increase due to equatorward advection of PV by the flow induced from the surface warm anomaly (Figure 6.18b, *thin solid line*).

From a height tendency (dynamic) perspective, we know from Figure 6.13 that pressure falls east of the upper PV blob due to advection of cyclonic QG PV by the ambient westerly shear. Moreover, an upward decrease in the cold-air advection to the west of the developing surface low pressure results in intensification of the upper-level low pressure. One may understand the development of surface high pressure upshear from the PV blob by similar reasoning.

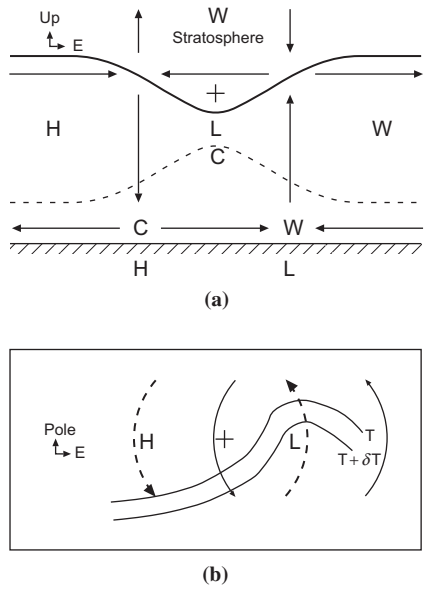

FIGURE 6.18 Schematic of quasi-geostrophic reasoning applied to extratropical cyclone development. (a) East–West vertical section showing the tropopause (*thick solid line*), the surface (*cross-hatched line*), a lower-tropospheric isentropic surface (*dashed line*), and the air circulations required to conserve potential vorticity for the typical case where westerly winds are increasing from the surface to the tropopause. Regions of relatively warm and cold air are given by "W" and "C," respectively, and regions of relatively low and high pressure are given by "L" and "H," respectively. (b) Horizontal plan view showing the surface isotherms (*solid lines*), surface wind associated with the upper-level PV disturbance (*thick dashed lines with arrows*), and surface wind associated with the surface cyclone (*thin solid lines with arrows*). In both (a) and (b), "+" shows the location of the PV disturbance due to the lowered tropopause. (*From Hakim, 2002.*)

From the *w* perspective, low-level vorticity increases east of the upper-level PV blob because of vortex stretching associated with rising air in the troposhpere above this location (Figure 6.18a, *arrows*). From Figure 6.15, we know that PV blobs in westerly shear produce ageostrophic circulations associated with this rising air and convergence near the surface, which increases the vorticity. From the thermodynamic energy equation, rising air tends to cool the column, partially canceling warming due to warm-air advection. By thickness reasoning, the warming over the surface low pressure is associated with an increase in the spacing between pressure surfaces so that, given a fixed upper surface in the lower stratosphere, the increased thickness is realized as a drop in the surface pressure. Again, one may understand the development of surface high pressure upshear from the PV blob by vortex squashing associated with sinking air.

We may now add the contributions of clouds and precipitation to this dry description of cyclogenesis. In the region of rising motion we expect clouds to form due to latent heat release. From the *w* perspective, this added heat helps

to intensify the developing cyclone by warming the column. From the PV-θ perspective, we must recognize that latent heating implies that PV is not conserved following air parcels, and from Section 4.4, we note that cyclonic PV is created below the level of maximum heating (see Figure 6.10a). This "new" PV is located above the surface cyclone, and as a result, produces a decrease in pressure and an increase in cyclonic circulation by PV inversion and superposition reasoning.

Finally, we note that the cyclogensis process is accelerated when the ambient static stability is reduced. This may be understood from the PV-θ perspective through an increase in the Rossby depth, which increases flow induced by the upper-level PV blob at the surface. From the w perspective, weaker static stability is also associated with a stronger and deeper ageostrophic circulation. Conversely, the cyclogenesis process is slowed for increasing ambient static stability. This is one reason why the main storm tracks for extratropical cyclones are found over the western margins of the Atlantic and Pacific oceans; the high heat capacity of the upper ocean allows relatively warm water in winter to heat the overlying lower atmosphere, weakening the static stability of the troposphere.

6.7 ISOBARIC FORM OF THE QG EQUATIONS

Gridded weather data and weather maps are typically available in isobaric, rather than constant height, surfaces. The reasons for this are partly historical, but also that density becomes implicit in the governing equations when pressure is used as a vertical coordinate. Nevertheless, using pressure as the vertical coordinate yields a "left-handed" coordinate system, since pressure increases down rather than up, which results in a more cumbersome interpretation of the equations. Upward vertical motion is negative in the isobaric system ($\omega = Dp/Dt$ is the vertical motion). Following is a summary of the QG equations in isobaric coordinates presented without proof. Interpretation of these equations is the same as for the height-coordinate counterparts presented earlier in the chapter, except here additional terms appear due to the inclusion of the β effect (the Coriolis parameter varies linearly with latitude); these are often small in magnitude, but are included here for completeness.

Hydrostatic balance is given by

$$\frac{\partial \Phi}{\partial p} = -\alpha = -RT/p \tag{6.57}$$

The geostrophic wind is defined by

$$\mathbf{V}_g \equiv f_0^{-1}\mathbf{k} \times \nabla_h \Phi \tag{6.58}$$

where Φ is the geopotential, and the β-plane approximation applies to the Coriolis parameter,

$$f = f_0 + \beta y \tag{6.59}$$

where f_0 is a constant, and $\beta \equiv (df/dy)_{\phi_0} = 2\Omega \cos\phi_0 / a$ and $y = 0$ at ϕ_0. The QG momentum equation takes the form

$$\frac{D_g \mathbf{V}_g}{Dt} = -f_0 \mathbf{k} \times \mathbf{V}_a - \beta y \mathbf{k} \times \mathbf{V}_g \tag{6.60}$$

and the QG mass continuity equation is

$$\frac{\partial u_a}{\partial x} + \frac{\partial v_a}{\partial y} + \frac{\partial \omega}{\partial p} = 0 \tag{6.61}$$

The adiabatic QG thermodynamic energy equation is

$$\left(\frac{\partial}{\partial t} + \mathbf{V}_g \cdot \nabla_h\right) T - \left(\frac{\sigma p}{R}\right) \omega = 0 \tag{6.62}$$

where $\sigma \equiv -RT_0 p^{-1} d\ln\theta_0/dp$ measures the static stability of the reference atmosphere. The QG vorticity equation is unchanged aside from the β term,

$$\frac{D_g \zeta_g}{Dt} = -f_0 \left(\frac{\partial u_a}{\partial x} + \frac{\partial v_a}{\partial y}\right) - \beta v_g \tag{6.63}$$

The vorticity–temperature-advection form of the QG height tendency equation ($\chi \equiv \partial\Phi/\partial t$),

$$\left[\nabla^2 + \frac{\partial}{\partial p}\left(\frac{f_0^2}{\sigma}\frac{\partial}{\partial p}\right)\right]\chi = -f_0 \mathbf{V}_g \cdot \nabla_h \left(\frac{1}{f_0}\nabla^2\Phi + f\right) - \frac{\partial}{\partial p}\left[-\frac{f_0^2}{\sigma}\mathbf{V}_g \cdot \nabla_h\left(-\frac{\partial\Phi}{\partial p}\right)\right] \tag{6.64}$$

includes advection of the planetary vorticity, as does the QG PV equation,

$$\left(\frac{\partial}{\partial t} + \mathbf{V}_g \cdot \nabla_h\right) q = \frac{D_g q}{Dt} = 0 \tag{6.65}$$

where the QG PV is given by

$$q \equiv \frac{1}{f_0}\nabla^2\Phi + f + \frac{\partial}{\partial p}\left(\frac{f_0}{\sigma}\frac{\partial\Phi}{\partial p}\right) \tag{6.66}$$

The Sutcliffe form of the QG omega (vertical motion) equation includes advection of the planetary vorticity

$$\left(\nabla^2 + \frac{f_0^2}{\sigma}\frac{\partial^2}{\partial p^2}\right)\omega \approx \frac{f_0}{\sigma}\left[\frac{\partial \mathbf{V}_g}{\partial p} \cdot \nabla_h\left(\frac{1}{f_0}\nabla^2\Phi + f\right)\right] \tag{6.67}$$

Finally, the **Q**-vector form of the QG omega (vertical motion) equation is

$$\sigma\,\nabla^2\omega + f_0^2\frac{\partial^2\omega}{\partial p^2} = -2\nabla \cdot \mathbf{Q} + f_0\beta\frac{\partial v_g}{\partial p} \tag{6.68}$$

where the **Q**-vector is given by

$$\mathbf{Q} \equiv (Q_1, Q_2) = \left(-\frac{R}{p} \frac{\partial \mathbf{V}_g}{\partial x} \cdot \nabla T, -\frac{R}{p} \frac{\partial \mathbf{V}_g}{\partial y} \cdot \nabla T \right) \tag{6.69}$$

SUGGESTED REFERENCES

Blackburn, *Interpretation of Ageostrophic Winds and Implications for Jetstream Maintenance,* discusses the differences between variable f(VF) and constant f(CF) ageostrophic motion.

Bluestein, *Synoptic-Dynamic Meteorology in Midlatitudes, Vol. II,* has a comprehensive treatment of midlatitude synoptic disturbances at the graduate level.

Cunningham and Keyser (2006) provide the theoretical basis for understanding jet streaks from a PV perspective.

Durran and Snellman (1987) illustrate the application of both traditional and **Q**-vector forms of the omega equation in diagnosing the vertical motion of an observed system.

Hakim, Cyclogenesis in *Encyclopedia of Atmospheric Sciences.*

Lackmann, *Midlatitude Synoptic Meteorology: Dynamics, Analysis, and Forecasting*, applies the quasi-geostrophic equations to the problem of weather analysis and forecasting.

Martin, *Mid-Latitude Atmospheric Dynamics: A First Course*, covers similar material as in this chapter, with an emphasis on the development of extratropical cyclones.

Pedlosky, *Geophysical Fluid Dynamics*, *2nd Edition,* presents a detailed formal derivation of the quasi-geostrophic system with applications to both the atmosphere and the oceans.

Vallis, *Atmospheric and Oceanic Fluid Dynamics: Fundamentals and Large-Scale Circulation,* presents a comprehensive treatment of the dynamics of both the atmosphere and ocean, including the quasi-geostrophic equations.

Wallace and Hobbs, *Atmospheric Science: An Introductory Survey,* has an excellent introductory-level description of the observed structure and evolution of midlatitude synoptic-scale disturbances.

PROBLEMS

6.1. Show that for a basic-state having linear shear, $\overline{U} = \lambda z$, λ constant, the basic-state QG PV depends only on z, and that the disturbance QG PV obeys

$$\left(\frac{\partial}{\partial t} + \overline{U} \frac{\partial}{\partial x} \right) q' = 0$$

6.2. Show that the Boussinesq continuity equation,

$$\frac{\partial u}{\partial x} + \frac{\partial v}{\partial y} + \frac{\partial w}{\partial z} = 0$$

can be written as

$$\frac{\partial u_a}{\partial x} + \frac{\partial v_a}{\partial y} + \frac{\partial w}{\partial z} = 0$$

where the subscript a indicates ageostrophic wind.

6.3. Prove identity (6.49).

6.4. In this problem you will derive an equation for the QG streamfunction of the ageostrophic secondary circulation. You should assume constant f and $\frac{d\overline{\theta}}{dz}$, and that the geostrophic flow is two-dimensional (y–z); specifically: $u_g = u_g(z, t)$ only and $v_g = v_g(y, t)$ only.

(a) Starting with geostrophic and hydrostatic balance,

$$\mathbf{V}_g = \frac{1}{\rho_0 f}\mathbf{k} \times \nabla_h p \qquad \frac{\partial p}{\partial z} = \frac{\rho_0 g}{\overline{\theta}}\theta$$

show that the maintenance of thermal wind balance requires

$$\frac{D}{Dt_g}\frac{\partial u_g}{\partial z} = -\frac{g}{\overline{\theta} f}\frac{D}{Dt_g}\frac{\partial \theta}{\partial y}$$

(b) Determine the left side of the result in (a) from the u_g momentum equation.

$$\frac{Du_g}{Dt_g} = f v_a$$

Interpret the result physically.

(c) Determine the right side of the result in (a) from the thermodynamic energy equation. Interpret the result physically.

(d) Now use your results from (b) and (c) in (a), using a streamfunction for the ageostrophic wind: $v_a = \frac{\partial \psi}{\partial z}$ and $w = -\frac{\partial \psi}{\partial y}$. Express your result with all streamfunction terms on the left side of the equation.

(e) Assume that the right side of your result in (d) reaches a local minimum in the midtroposphere. Sketch the ageostrophic circulation streamlines in a y–z cross-section along with arrows showing v_a and w.

6.5. Consider two spherical, cyclonic QG PV anomalies. One anomaly is located at the origin and has unity radius. The second anomaly is located at $(x, y, z) = (2, 0, 0)$ and has radius and amplitude one-half the corresponding values of the other anomaly. Draw an (x, y) sketch estimating the trajectory traced out by these two anomalies assuming that their shape is preserved. Draw a second sketch showing the w field at a level above the anomalies.

6.6. **(a)** Derive the dispersion relationship for 3D QG Rossby waves on the β-plane. Assume plane waves in the absence of mean flow and boundaries. The governing (disturbance PV) equation is modified by an additional term

$$\frac{Dq}{Dt_g} + v\beta = 0$$

(b) Derive the group velocity vector. Explain the result.

6.7. Derive the QG kinetic energy equation

$$\frac{\partial K}{\partial t_g} + \nabla \cdot \vec{S} = \frac{g}{\theta_0} w\theta$$

starting with the QG momentum equation

$$\frac{D\mathbf{V}_g}{Dt_g} = -f\mathbf{k} \times \vec{V}_a$$

6.8. We have considered simple PV distributions associated with points and spheres. Now consider an extremely complicated PV structure, which is completely contained within a cube having sides of length L. Without knowing the detailed structure of the PV, derive a formula relating the circulation on the lateral sides of the cube, and the mean θ on the top and bottom of the cube, to the mean PV in the cube. [*Hint*: First show that the QG PV can be expressed as the divergence of a vector field.]

MATLAB Exercises

M6.1. Examine the impact of disturbance horizontal scale using the idealized QG PV inversion routine **QG_PV_inversion.m**. Use the parallelpiped initial condition ($ipv = 1$) with an amplitude of 2 PVU. Make a plot of how the disturbance minimum pressure changes as a function of the size of the disturbance (controlled by the parameter *iw* in the routine **QG_initial_value.m**). Repeat the exercise using a Dirichlet boundary condition (zero surface pressure; set $idn = -1$) and compare your results to the Neumann case. Repeat the exercise again by moving the boundaries very far apart (set *ZH* to 10 in **grid_setup.m**). Compare the pressure of all three solutions at a fixed distance below the PV anomaly (e.g., 5.5 km below the anomaly). What can you conclude about the sensitivity to boundary conditions for the Neumann and Dirichlet cases?

M6.2. Set the disturbance in the idealized QG PV inversion routine **QG_PV_inversion.m** to a jet streak ($ipv = 5$) with an amplitude of 2 PVU. Compute the wind speed and make a plot of the wind speed and wind vectors (using *quiver*). Make a blocking pattern by changing the sign on the QG PV amplitude variable *pvmag* so that the dipole pattern reverses. Make a plot of wind speed and wind vectors including a constant zonal wind so that the total zonal wind speed between the vortices is zero. Perform piecewise QG PV inversion on the cyclonic and anticyclone vortices in isolation and, including the constant zonal wind, use PV Thinking to explain why the blocking pattern does not move.

M6.3. The code **QG_model.m** is a numerical solver of the quasi-geostrophic equations in $PV - \theta$ form. Initialize the model with a "blob" of PV ($ipv = 4$) in a simple linear-shear jet ($ijet = 1$). Run the model for 96 hours. Use the plotting code **plot_QG_model.m** to create figures for the solution at various times. Diagnose the solution using **QG_diagnostics.m**. From the solutions of the height tendency equation, describe the evolution of the surface pressure field. From the diagnosed vertical motion field, diagnose the vortex stretching term in the vorticity equation, and use the result to describe the evolution of the surface geostrophic vorticity field. Finally, one might expect the PV blob to tilt over in the linear shear. Check to see if this happens, and explain what you find.

M6.4. For the solution in problem M6.3, solve for the rotational ageostrophic wind defined by (6.22) with $p_a = 0$. Since this component of the wind has no divergence, we may express it in terms of a streamfuntion

$$\mathbf{V}_a = \mathbf{k} \times \nabla \psi_a \tag{6.70}$$

Derive an expression for the ageostrophic vorticity from (6.70) that can be used in (6.22). Plot the rotational ageostrophic wind using *quiver* at the level of the blob along with the pressure field. The sum of the geostrophic and the total ageostrophic wind (rotational plus divergent) provides the QG estimate of the gradient wind. How do the results compare with your expectations based on Section 3.2.5?

M6.5. Initialize **QG_model.m** with a blocking configuration (dipole with high PV over low PV) for the PV described in Problem M6.2. Use **QG_diagnostics.m** to determine favored locations for cloud and precipitation. How does the w pattern compare with a jet streak? Add a constant wind to the linear shear using parameter *Unot*, and note that your value should be non-dimensionalized using the scaling parameter, U. Pick a value for *Unot* that makes the block stationary. Next, average the QG PV and boundary potential temperature fields for the last few output times, and use the result as the initial condition for a new experiment with the value of *Unot* that makes the pattern stationary. How does the result differ from the first experiment? Repeat the experiment by adding a small-amplitude random field to the initial condition. What does the result tell you about why blocks are so persistent in the atmosphere?